arXiv:1903.11661v2 [hep-ph] 8 May 2019

A 96 GeV Higgs Boson in the N2HDM

T. Biekötter,[1,2] **M. Chakraborti,**[1] **S.Heinemeyer**[1,3,4]

[1]*Instituto de Física Teórica UAM-CSIC, Cantoblanco, 28049, Madrid, Spain*

[2]*Departamento de Física Teórica, Universidad Autónoma de Madrid (UAM), Campus de Cantoblanco, 28049 Madrid, Spain*

[3]*Campus of International Excellence UAM+CSIC, Cantoblanco, 28049, Madrid, Spain*

[4]*Instituto de Física de Cantabria (CSIC-UC), 39005, Santander, Spain*

E-mail: thomas.biekotter@csic.es, mani.chakraborti@gmail.com, Sven.Heinemeyer@cern.ch

ABSTRACT: We discuss a $\sim 3\,\sigma$ signal (local) in the light Higgs-boson search in the diphoton decay mode at ~ 96 GeV as reported by CMS, together with a $\sim 2\,\sigma$ excess (local) in the $b\bar{b}$ final state at LEP in the same mass range. We interpret this possible signal as a Higgs boson in the 2 Higgs Doublet Model with an additional real Higgs singlet (N2HDM). We find that the lightest Higgs boson of the N2HDM can perfectly fit both excesses simultaneously, while the second lightest state is in full agreement with the Higgs-boson measurements at 125 GeV, and the full Higgs-boson sector is in agreement with all Higgs exclusion bounds from LEP, the Tevatron and the LHC as well as other theoretical and experimental constraints. We show that only the N2HDM type II and IV can fit both the LEP excess and the CMS excess with a large ggF production component at ~ 96 GeV. We derive bounds on the N2HDM Higgs sector from a fit to both excesses and describe how this signal can be further analyzed at the LHC and at future e^+e^- colliders, such as the ILC.

Contents

1 Introduction

In the year 2012 the ATLAS and CMS collaborations have discovered a new particle that – within theoretical and experimental uncertainties – is consistent with the existence of a Standard-Model (SM) Higgs boson at a mass of $\sim$ 125 GeV [1–3]. No conclusive signs of physics beyond the SM have been found so far at the LHC. However, the measurements of Higgs-boson couplings, which are known experimentally to a precision of roughly $\sim$ 20%, leave room for Beyond Standard-Model (BSM) interpretations. Many BSM models possess extended Higgs-boson sectors. Consequently, one of the main tasks of the LHC Run II and beyond is to determine whether the observed scalar boson forms part of the Higgs sector of an extended model. Extended Higgs-boson sectors naturally contain additional Higgs bosons with masses larger than 125 GeV.

However, many extensions also offer the possibilty of additional Higgs bosons *lighter* than 125 GeV. Consequently, the search for lighter Higgs bosons forms an important part in the BSM Higgs-boson analyses.

Searches for Higgs bosons below 125 GeV have been performed at LEP, the Tevatron and the LHC. LEP reported a $2.3\,\sigma$ local excess observed in the $e^+e^- \to Z(H \to b\bar{b})$ searches [4], which would be consistent with a scalar of mass ~ 98 GeV, but due to the $b\bar{b}$ final state the mass resolution is rather coarse). The excess corresponds to

$$\mu_{\mathrm{LEP}} = \frac{\sigma\left(e^+e^- \to Z\phi \to Zb\bar{b}\right)}{\sigma^{\mathrm{SM}}\left(e^+e^- \to ZH \to Zb\bar{b}\right)} = 0.117 \pm 0.057 \,, \tag{1.1}$$

where the signal strength μ_{LEP} is the measured cross section normalized to the SM expectation, with the SM Higgs-boson mass at ~ 98 GeV. The value for μ_{LEP} was extracted in Ref. [5] using methods described in Ref. [6].

Interestingly, recent CMS Run II results [7] for Higgs-boson searches in the diphoton final state show a local excess of $\sim 3\,\sigma$ around ~ 96 GeV, with a similar excess of $2\,\sigma$ in the Run I data at a comparable mass [8]. In this case the excess corresponds to (combining 7, 8 and 13 TeV data, and assuming that the gg production dominates)

$$\mu_{\mathrm{CMS}} = \frac{\sigma\left(gg \to \phi \to \gamma\gamma\right)}{\sigma^{\mathrm{SM}}\left(gg \to H \to \gamma\gamma\right)} = 0.6 \pm 0.2 \,. \tag{1.2}$$

First Run II results from ATLAS with $80\,\mathrm{fb}^{-1}$ in the $\gamma\gamma$ searches below 125 GeV were recently published [9]. No significant excess above the SM expectation was observed in the mass range between 65 and 110 GeV. However, the limit on cross section times branching ratio obtained in the diphoton final state by ATLAS is not only well above μ_{CMS}, but even weaker than the corresponding upper limit obtained by CMS at $\sim$ 96 GeV. This was illustrated in Fig. 1 in Ref. [10].

Since the CMS and the LEP excesses in the light Higgs-boson searches are found effectively at the same mass, this gives rise to the question whether they might be of a common origin – and if there exists a model which could explain the two excesses simultaneously, while being in agreement with all other Higgs-boson related limits and measurements. A review about these possibilities was given in Refs. [10, 11]. The list comprises of type I 2HDMs [12, 13], a radion model [14], a minimal dilaton model [15], as well as supersymmetric models [16–18].

Motivated by the Hierarchy Problem, Supersymmetric extensions of the SM play a prominent role in the exploration of new physics. Supersymmetry (SUSY) doubles the particle degrees of freedom by predicting two scalar partners for all SM fermions, as well as fermionic partners to all SM bosons. The simplest SUSY extension of the

SM is the Minimal Supersymmetric Standard Model (MSSM) [19, 20]. In contrast to the single Higgs doublet of the SM, the MSSM by construction, requires the presence of two Higgs doublets, Φ_1 and Φ_2. In the $\mathcal{CP}$ conserving case the MSSM Higgs sector consists of two $\mathcal{CP}$-even, one $\mathcal{CP}$-odd and two charged Higgs bosons. The light (or the heavy) $\mathcal{CP}$-even MSSM Higgs boson can be interpreted as the signal discovered at ~ 125 GeV [21] (see Refs. [22, 23] for recent updates). However, in Ref. [22] it was demonstrated that the MSSM cannot explain the CMS excess in the diphoton final state.

Going beyond the MSSM, a well-motivated extension is given by the Next-to-MSSM (NMSSM) (see [24, 25] for reviews). The NMSSM provides a solution for the so-called "μ problem" by naturally associating an adequate scale to the μ parameter appearing in the MSSM superpotential [26, 27]. In the NMSSM a new singlet superfield is introduced, which only couples to the Higgs- and sfermion-sectors, giving rise to an effective μ-term, proportional to the vacuum expectation value (vev) of the scalar singlet. In the $\mathcal{CP}$ conserving case the NMSSM Higgs sector consists of three $\mathcal{CP}$-even Higgs bosons, h_i ($i = 1, 2, 3$), two $\mathcal{CP}$-odd Higgs bosons, a_j ($j = 1, 2$), and the charged Higgs boson pair $H^\pm$. In the NMSSM not only the lightest but also the second lightest $\mathcal{CP}$-even Higgs boson can be interpreted as the signal observed at about 125 GeV, see, e.g., [28, 29]. In Ref. [17] it was found that the NMSSM can indeed simultaeneously satisfy the two excesses mentioned above. In this case, the Higgs boson at ~ 96 GeV has a large singlet component, but also a sufficiently large doublet component to give rise to the two excesses.

A natural extension of the NMSSM is the $\mu\nu$SSM, in which the singlet superfield is interpreted as a right-handed neutrino superfield [30, 31] (see Refs. [32–34] for reviews). The $\mu\nu$SSM is the simplest extension of the MSSM that can provide massive neutrinos through a see-saw mechanism at the electroweak scale. A Yukawa coupling for right-handed neutrinos of the order of the electron Yukawa coupling is introduced that induces the explicit breaking of R-parity. Also in the $\mu\nu$SSM the signal at ~ 125 GeV can be interpreted as the lightest or the second lightest $\mathcal{CP}$-even scalar. In Ref. [16] the "one generation case" (only one generation of massive neutrinos) was analyzed: within the scalar sector, due to R-parity breaking, the left- and right-handed sneutrinos mix with the doublet Higgses and form six massive $\mathcal{CP}$-even and five massive $\mathcal{CP}$-odd states, assuming that there is no $\mathcal{CP}$-violation. However, due to the smallness of R-parity breaking in the $\mu\nu$SSM, the mixing of the doublet Higgses with the left-handed sneutrinos is very small. Consequently, in the one-generation case the Higgs-boson sector of the $\mu\nu$SSM, i.e. the $\mathcal{CP}$-even/odd Higgs doublets and the $\mathcal{CP}$-even/odd right handed sneutrino, resembles the Higgs-boson sector in the NMSSM. In Ref. [16] it was found that also the $\mu\nu$SSM can fit the CMS and the LEP excesses simultaneously. In this

case the scalar at ~ 96 GeV has a large right-handed sneutrino component. The three generation case (i.e. with three generations of massive neutrinos) is currently under investigation [35].

Motivated by the fact that two models with two Higgs doublets and (effectively) one Higgs singlet can fit the CMS excess in Eq. (1.2) and the LEP excess in Eq. (1.1), we investigate in this work the Next to minimal two Higgs doublet model (N2HDM) [36, 37]. Similar to the above two models, in N2HDM the two Higgs doublets are supplemented with a real Higgs singlet, giving rise to one additional (potentially light) $\mathcal{CP}$-even Higgs boson. However, in comparison with the NMSSM and the $\mu\nu$SSM the N2HDM does not have to obey the SUSY relations in the Higgs-boson sector. Consequently, it allows to study how the potential fits the two excesses simultaneously in a more general way. Our paper is organized as follows. In Sect. 2 we describe the relevant features of the N2HDM. The experimental and theoretical constraints taken into account are given in Sect. 3. Details about the experimental excesses as well as how we implement them are summarized in Sect. 4. In Sect. 5 we show our results in the different versions of the N2HDM and discuss the possibilities to investigate these scenarios at current and future colliders. We conclude with Sect. 6.

2   The model: N2HDM

The N2HDM is the simplest extension of a $\mathcal{CP}$-conserving two Higgs doublet model (2HDM) in which the latter is augmented with a real scalar singlet Higgs field. The scalar potential of this model can be given as [36, 37]

$$
\begin{aligned}
V = {} & m_{11}^2|\Phi_1|^2 + m_{22}^2|\Phi_2|^2 - m_{12}^2(\Phi_1^\dagger\Phi_2 + h.c.) + \frac{\lambda_1}{2}(\Phi_1^\dagger\Phi_1)^2 + \frac{\lambda_2}{2}(\Phi_2^\dagger\Phi_2)^2 \\
& + \lambda_3(\Phi_1^\dagger\Phi_1)(\Phi_2^\dagger\Phi_2) + \lambda_4(\Phi_1^\dagger\Phi_2)(\Phi_2^\dagger\Phi_1) + \frac{\lambda_5}{2}[(\Phi_1^\dagger\Phi_2)^2 + h.c.] \\
& + \frac{1}{2}m_S^2\Phi_S^2 + \frac{\lambda_6}{8}\Phi_S^4 + \frac{\lambda_7}{2}(\Phi_1^\dagger\Phi_1)\Phi_S^2 + \frac{\lambda_8}{2}(\Phi_2^\dagger\Phi_2)\Phi_S^2 \,,
\end{aligned}
\tag{2.1}
$$

where Φ_1 and Φ_2 are the two $SU(2)_L$ doublets whereas Φ_S is a real scalar singlet. To avoid the occurrence of tree-level flavor changing neutral currents (FCNC), a Z_2 symmetry is imposed on the scalar potential of the model under which the scalar fields transform as

$$
\Phi_1 \to \Phi_1 \,, \quad \Phi_2 \to -\Phi_2 \,, \quad \Phi_S \to \Phi_S \,.
\tag{2.2}
$$

This Z_2, however, is softly broken by the m_{12}^2 term in the Lagrangian. The extension of the Z_2 symmetry to the Yukawa sector forbids tree-level FCNCs. As in the 2HDM, one

	u-type	d-type	leptons
type I	Φ_2	Φ_2	Φ_2
type II	Φ_2	Φ_1	Φ_1
type III (lepton-specific)	Φ_2	Φ_2	Φ_1
type IV (flipped)	Φ_2	Φ_1	Φ_2

Table 1. Allowed fermion couplings in the four types of N2HDM.

can have four variants of the N2HDM, depending on the Z_2 parities of the fermions. Tab. 1 lists the couplings for each type of fermion allowed by the Z_2 parity in four different types of N2HDM.

Taking the electroweak symmetry breaking (EWSB) minima to be charge and $\mathcal{CP}$-conserving, the scalar fields after EWSB can be parametrised as

$$\Phi_1 = \begin{pmatrix} \phi_1^+ \\ \frac{1}{\sqrt{2}}(v_1 + \rho_1 + i\eta_1) \end{pmatrix} , \quad \Phi_2 = \begin{pmatrix} \phi_2^+ \\ \frac{1}{\sqrt{2}}(v_2 + \rho_2 + i\eta_2) \end{pmatrix} , \quad \Phi_S = v_S + \rho_S , \quad (2.3)$$

where v_1, v_2, v_S are the real vevs acquired by the fields Φ_1, Φ_2 and Φ_S respectively. As in the 2HDM we define $\tan\beta := v_2/v_1$. As is evident from Eq. (2.3), under such a field configuration, the $\mathcal{CP}$-odd and charged Higgs sector of the N2HDM remain completely unaltered with respect to its 2HDM counterpart. However, the $\mathcal{CP}$-even scalar sector can undergo significant changes due the mixing among ρ_1, ρ_2 and ρ_S, leading to a total of three $\mathcal{CP}$-even physical Higgses. Thus, a rotation from the interaction to the physical basis can be achieved with the help of a 3×3 orthogonal matrix as

$$\begin{pmatrix} h_1 \\ h_2 \\ h_3 \end{pmatrix} = R \begin{pmatrix} \rho_1 \\ \rho_2 \\ \rho_S \end{pmatrix} . \quad (2.4)$$

We use the convention $m_{h_1} < m_{h_2} < m_{h_3}$ throughout the paper. The rotation matrix R can be parametrized as

$$R = \begin{pmatrix} c_{\alpha_1} c_{\alpha_2} & s_{\alpha_1} c_{\alpha_2} & s_{\alpha_2} \\ -(c_{\alpha_1} s_{\alpha_2} s_{\alpha_3} + s_{\alpha_1} c_{\alpha_3}) & c_{\alpha_1} c_{\alpha_3} - s_{\alpha_1} s_{\alpha_2} s_{\alpha_3} & c_{\alpha_2} s_{\alpha_3} \\ -c_{\alpha_1} s_{\alpha_2} c_{\alpha_3} + s_{\alpha_1} s_{\alpha_3} & -(c_{\alpha_1} s_{\alpha_3} + s_{\alpha_1} s_{\alpha_2} c_{\alpha_3}) & c_{\alpha_2} c_{\alpha_3} \end{pmatrix} , \quad (2.5)$$

$\alpha_1, \alpha_2, \alpha_3$ being the three mixing angles, and we use the short-hand notation $s_x = \sin x$, $c_x = \cos x$. The singlet admixture of each physical state can be computed as $\Sigma_{h_i} = |R_{i3}|^2, i = 1, 2, 3$. The couplings of the Higgs bosons to SM particles are modified

w.r.t. the SM Higgs-coupling predictions due to the mixing in the Higgs sector. It is convenient to express the couplings of the scalar mass eigenstates h_i normalized to the corresponding SM couplings. We therefore introduce the coupling coefficients $c_{h_i VV}$ and $c_{h_i f \bar{f}}$, such that the couplings to the massive vector bosons are given by

$$(g_{h_i WW})_{\mu\nu} = \mathrm{i} g_{\mu\nu} \left(c_{h_i VV} \right) g M_W \quad \text{and} \quad (g_{h_i ZZ})_{\mu\nu} = \mathrm{i} g_{\mu\nu} \left(c_{h_i VV} \right) \frac{g M_Z}{c_{\mathrm{w}}}, \qquad (2.6)$$

where g is the $SU(2)_L$ gauge coupling, c_{w} the cosine of weak mixing angle, $c_{\mathrm{w}} = M_W / M_Z, s_{\mathrm{w}} = \sqrt{1 - c_{\mathrm{w}}^2}$, and M_W and M_Z the masses of the W boson and the Z boson, respectively. The couplings of the Higgs bosons to the SM fermions are given by

$$g_{h_i f \bar{f}} = \frac{m_f}{v} \left(c_{h_i f \bar{f}} \right), \qquad (2.7)$$

where m_f is the mass of the fermion and $v = \sqrt{(v_1^2 + v_2^2)}$ is the SM vev. In Tab. 2 we list the coupling coefficients for the couplings to gauge bosons $V = W, Z$ for the three $\mathcal{CP}$-even Higgses. They are identical in all four types of the (N)2HDM. The same for the couplings to the fermions is listed in Tab. 3 for the four types of the N2HDM. One can observe from Tab. 3 that the coupling pattern of the Yukawa sector in N2HDM is the same as that of 2HDM.

From Eq. (2.1), one can see that there are altogether 12 independent parameters in the model,

$$m_{11}^2, \quad m_{22}^2, \quad m_{12}^2, \quad m_S^2, \quad \lambda_{i, \; i=1,8}. \qquad (2.8)$$

However, one can use the three minimization conditions of the potential at the vacuum to substitute the bilinears m_{11}^2, m_{22}^2 and m_S^2 for v, $\tan\beta$ and v_S. Furthermore, the quartic couplings λ_i can be replaced by the physical scalar masses and mixing angles, leading to the following parameter set [37];

$$\alpha_{1,2,3}, \quad \tan\beta, \quad v, \quad v_S, \quad m_{h_{1,2,3}}, \quad m_A, \quad M_{H^\pm}, \quad m_{12}^2, \qquad (2.9)$$

where m_A, $M_{H^\pm}$ denote the masses of the physical $\mathcal{CP}$-odd and charged Higgses respectively. We use the code `ScannerS` [37, 38] in our analysis to uniformly explore the set of independent parameters as given in Eq. (2.9) (see below).

In our analysis we will identify the lightest $\mathcal{CP}$-even Higgs boson, h_1, with the one being potentially responsible for the signal at ~ 96 GeV. The second lightest $\mathcal{CP}$-even Higgs boson will be identified with the one observed at ~ 125 GeV.

3   Relevant constraints

In this section we will describe the various theoretical and experimental constraints considered in our scans. The theoretical constraints are all implemented in `ScannerS`.

$c_{h_i VV} = c_\beta R_{i1} + s_\beta R_{i2}$
h_1 $\quad c_{\alpha_2} c_{\beta-\alpha_1}$
h_2 $\quad -c_{\beta-\alpha_1} s_{\alpha_2} s_{\alpha_3} + c_{\alpha_3} s_{\beta-\alpha_1}$
h_3 $\quad -c_{\alpha_3} c_{\beta-\alpha_1} s_{\alpha_2} - s_{\alpha_3} s_{\beta-\alpha_1}$

Table 2. The coupling factors of the neutral $\mathcal{CP}$-even Higgs bosons h_i to the massive gauge bosons $V = W, Z$ in the N2HDM.

	u-type $(c_{h_i t\bar{t}})$	d-type $(c_{h_i b\bar{b}})$	leptons $(c_{h_i \tau\bar{\tau}})$
type I	R_{i2}/s_β	R_{i2}/s_β	R_{i2}/s_β
type II	R_{i2}/s_β	R_{i1}/c_β	R_{i1}/c_β
type III (lepton-specific)	R_{i2}/s_β	R_{i2}/s_β	R_{i1}/c_β
type IV (flipped)	R_{i2}/s_β	R_{i1}/c_β	R_{i2}/s_β

Table 3. Coupling factors of the Yukawa couplings of the N2HDM Higgs bosons h_i w.r.t. their SM values.

For more details, we refer the reader to the corresponding references given below. The experimental constraints implemented in `ScannerS` were supplemented with the most recent ones by linking the parameter points from `ScannerS` to the more recent versions of other public codes, which we will also describe in more detail in the following.

3.1 Theoretical constraints

Like all models with extended scalar sectors, the N2HDM also faces important constraints coming from tree-level perturbartive unitarity, stability of the vacuum and the condition that the vacuum should be a global minimum of the potential. We briefly describe these constraints below.

- Tree-level perturbative unitarity conditions ensure that the potential remains perturbative up to very high energy scales. This is achieved by demanding that the amplitudes of the scalar quartic interactions leading to $2 \to 2$ scattering processes remain below the value of 8π at tree-level. The calculation was carried out in Ref. [37] and is implemented in `ScannerS`.

- Boundedness from below demands that the potential remains positive when the field values approach infinity. `ScannerS` automatically ensures that the N2HDM potential is bounded from below by verifying that the necessary and sufficient conditions as given in Ref. [39] are fulfilled. The same conditions can be found in Ref. [37] in the notation adopted in this paper.

- Following the procedure of `ScannerS`, we impose the condition that the vacuum should be a global minimum of the potential. Although this condition can be avoided in the case of a metastable vacuum with the tunneling time to the real minimum being larger than the age of the universe, we do not explore this possibility in this analysis. Details on the algorithm implemented in `ScannerS` to find the global minimum of the potential can be found in Ref. [38]. This algorithm has the advantage that it works with the scalar masses and vevs as independent set of parameters, which can be directly related to physical observables. It also finds the global minimum of the potential without having to solve coupled non-linear equations, therefore avoiding the usually numerically most expensive task in solving the stationary conditions.

3.2 Constraints from direct searches at colliders

Searches for charged Higgs bosons at the LHC are very effective constraining the $\tan\beta$-$M_{H^\pm}$ plane of 2HDMs [40]. Since the charged scalar sector of the 2HDM is identical to that of the N2HDM, the bounds on the parameter space of the former also cover the corresponding parameter space of the latter. Important searches in our context are the direct charged Higgs production $pp \to H^\pm tb$ with the decay modes $H^\pm \to \tau\nu$ and $H^\pm \to tb$ [41]. The 95% confidence level exclusion limits of all important searches for charged Higgs bosons are included in the public code `HiggsBounds v.5.3.2` [42–46]. The theoretical cross section predictions for the production of the charged Higgs at the LHC are provided by the LHC Higgs Cross Section Working Group [47–50].[1] The rejected parameter points are concentrated in the region $\tan\beta < 1$, where the coupling of the charged Higgs to top quarks is enhanced [41]. Bounds from searches for charged Higgs bosons at LEP [51–57] are irrelevant for our analysis, because constrains from flavor physics observables usually exclude very light $H^\pm$ kinematically in the reach of LEP.

Direct searches for additional neutral Higgs bosons can exclude some of the parameter points, mainly when the heavy Higgs boson h_3 or the $\mathcal{CP}$-odd Higgs boson A are rather light. `HiggsBounds` includes all relevant LHC searches for additional Higgs bosons, such as possible decays of h_3 and A to the singlet-like state h_1 or the SM-like Higgs boson h_2. The most relevant channels are the following: CMS searched for pseudoscalars decaying into a Z-boson and scalar in final states with two b-jets and two leptons, where the scalar lies in the mass range of 125 ± 10 GeV [58, 59]. Both ATLAS and CMS searched for additional heavy Higgs bosons in the $H \to ZZ$ decay

---

[1]We thank T. Stefaniak for a program to extract the prediction from the grid provided by the LHC Higgs Cross Section Working Group.

channel including different final states [60–62]. For the flipped scenario, apart from the searches just mentioned, also the search for $\mathcal{CP}$-even and -odd scalars decaying into a Z-boson and a scalar, which then decays to a pair of τ-leptons [63], is relevant, because the coupling of the light singlet-like scalar at ~ 96 GeV to τ-leptons can be enhanced. Of course, the light scalar is also directly constrained via the Higgsstrahlung process with subsequent decay to a pair of b-quarks at LEP [64] and by searches for diphoton resonances at the LHC including all relevant production mechanisms [7, 9]. However, these constraints are weak, and they are the ones where LEP and CMS saw the excesses we are investigating here.

3.3 Constraints from the SM-like Higgs-boson properties

Any model beyond the SM has to accommodate the SM-like Higgs boson, with mass and signal strengths as they were measured at the LHC [1–3]. In our scans the compatibility of the $\mathcal{CP}$-even scalar h_2 with a mass of 125.09 GeV with the measurements of signal strengths at Tevatron and LHC is checked in a twofold way.

Firstly, the program `ScannerS`, that we use to generate the benchmark points, contains an individual check of the signal strengths

$$\frac{\mu_F}{\mu_V} \;, \quad \mu_F^{\gamma\gamma} \;, \quad \mu_F^{ZZ} \;, \quad \mu_F^{WW} \;, \quad \mu_F^{\tau\tau} \;, \quad \mu_F^{bb} \;, \tag{3.1}$$

as they are quoted in Ref. [3], where an agreement within $\pm 2\,\sigma$ is required. The signal strengths are defined as

$$\mu_F^{xx} = \mu_F \frac{\mathrm{BR}_{\mathrm{N2HDM}}(h_i \to xx)}{\mathrm{BR}_{\mathrm{SM}}(H \to xx)} \;. \tag{3.2}$$

Here, the production cross sections associated with couplings to fermions, normalized to the SM prediction, are defined as

$$\mu_F = \frac{\sigma_{\mathrm{N2HDM}}(\mathrm{ggF}) + \sigma_{\mathrm{N2HDM}}(\mathrm{bbH})}{\sigma_{\mathrm{SM}}(\mathrm{ggF})} \;, \tag{3.3}$$

where the production in association with a pair of b-quarks (bbH) can be neglected in the SM, whereas in N2HDM it has to be included since it can be enhanced by $\tan\beta$. The cross section for vector boson fusion (VBF) production and the associated production with a vector boson (VH) are given by the coupling coefficient c_{h_2VV},

$$\mu_V = \frac{\sigma_{\mathrm{N2HDM}}(\mathrm{VBF})}{\sigma_{\mathrm{SM}}(\mathrm{VBF})} = \frac{\sigma_{\mathrm{N2HDM}}(VH)}{\sigma_{\mathrm{SM}}(VH)} = c_{h_2VV}^2 \;, \tag{3.4}$$

where we made use of the fact that QCD corrections cancel in the ratio of the vector boson fusion cross sections in the N2HDM and the SM [37]. The ggF and bbH cross

sections are provided by `ScannerS` with the help of data tables obtained using the public code `SusHi` [65, 66]. The couplings squared normalized to the SM prediction, for instance $c^2_{h_i VV}$, are calculated via the interface of `ScannerS` with the spectrum generator `N2HDECAY` [37, 67, 68].

In a second step, we supplemented the Higgs-boson data from Ref. [3] that is implemented in `ScannerS` with the most recent Higgs-boson measurements: we verify the agreement of the generated points with all currently available measurements using the public code `HiggsSignals v.2.2.3` [69–71]. `HiggsSignals` provides a statistical χ^2 analysis of the SM-like Higgs-boson predictions of a certain model compared to the measurement of Higgs-boson signal rates and masses from Tevatron and LHC. The complete list of implemented experimental data can be found in Ref. [72]. In our scans, we will show the reduced χ^2,

$$\chi^2_{\rm red} = \frac{\chi^2}{n_{\rm obs}} \, , \tag{3.5}$$

where χ^2 is provided by `HiggsSignals` and $n_{\rm obs} = 101$ is the number of experimental observations considered.

3.4 Constraints from flavor physics

Constraints from flavor physics prove to be very significant in the N2HDM because of the presence of the charged Higgs boson. Since the charged Higgs sector of N2HDM is unaltered with respect to 2HDM, we can translate the bounds from the 2HDM parameter space directly on to our scenario for most of the observables. Various flavor observables like rare B decays, B meson mixing parameters, $\mathrm{BR}(B \to X_s \gamma)$, LEP constraints on Z decay partial widths etc., which are sensitive to charged Higgs boson exchange, provide effective constraints on the available parameter space [40, 73]. However, for the low $\tan\beta$ region that we are interested in (see below), the constraints which must be taken into account are [40]: $\mathrm{BR}(B \to X_s \gamma)$, constraints on ΔM_{B_s} from neutral $B-$meson mixing and $\mathrm{BR}(B_s \to \mu^+ \mu^-)$. The dominant contributions to the former two processes come from diagrams involving $H^\pm$ and top quarks (see e.g. Refs. [74–76] for $\mathrm{BR}(B \to X_s \gamma)$ and Refs. [77–79] for ΔM_{B_s}) and can be taken to be independent of the neutral scalar sector to a very good approximation. Thus, the bounds for them can be taken over directly from the 2HDM to our case. Since the $H^\pm t b$ coupling depends on the Yukawa sector of the model, the flavor bounds can differ for different N2HDM types [40]. Owing to identical quark Yukawa coupling patterns, limits for type I and III scenarios come out to be very similar. The same holds for type II and IV. Constraints from $\mathrm{BR}(B \to X_s \gamma)$ exclude $M_{H^\pm} < 650$ GeV for all values of $\tan\beta \gtrsim 1$ in the type II and IV 2HDM, while for type I and III the bounds are more $\tan\beta-$dependent. For

$M_{H^\pm} \geq 650$ GeV (as in our case) the dominant constraint is the one obtained from the measurement of ΔM_{B_s}.

For still lower values of $\tan\beta \lesssim 1$, bounds from the measurement of BR($B_s \to \mu^+\mu^-$) become important [40]. Unlike the above two observables, BR($B_s \to \mu^+\mu^-$) can get contributions from the neutral scalar sector of the model as well [80, 81]. Thus, in principle the value of BR($B_s \to \mu^+\mu^-$) in the N2HDM may differ from that of 2HDM because of additional contributions coming from h_1 containing a large singlet component (see below). However, we must note that the contributions from the N2HDM $\mathcal{CP}$-even Higgs bosons can be expected to be small once we demand the presence of substantial singlet components in them, as it is the case in our analysis. A detailed calculation of various flavor observables in the specific case of the N2HDM is beyond the scope of this work. Furthermore, as mentioned in Sect. 3.2, in the region $\tan\beta \lesssim 1$, the constraints from direct LHC searches of $H^\pm$ already provide fairly strong constraints. Also the constraint from ΔM_{B_s} covers the region of very small $\tan\beta$. Keeping the above facts in mind, in our work we use the flavor bounds for BR($B \to X_s\gamma$) and ΔM_{B_s} as obtained in Ref. [40] for different N2HDM types.

3.5 Constraints from electroweak precision data

Constraints from electroweak precision observables can in a simple approximation be expressed in terms of the oblique parameters S, T and U [82, 83]. Deviations to these parameters are significant if new physics beyond the SM enters mainly through gauge boson self-energies, as it is the case for extended Higgs sectors. ScannerS has implemented the one-loop corrections to the oblique parameters for models with an arbitrary number of Higgs doublets and singlets from Ref. [84]. This calculation is valid under the criteria that the gauge group is the SM $SU(2) \times U(1)$, and that particles beyond the SM have suppressed couplings to light SM fermions. Both conditions are fulfilled in the N2HDM. Under these assumptions, the corrections are independent of the Yukawa sector of the N2HDM, and therefore the same for all types. The corrections to the oblique parameters are very sensitive to the relative mass squared differences of the scalars. They become small when either the heavy doublet-like Higgs h_3 or the $\mathcal{CP}$-odd scalar A have a mass close to the mass of the charged Higgs boson [85, 86]. In 2HDMs there is a strong correlation between T and U, and T is the most sensitive of the three oblique parameters. Thus, U is much smaller in points not excluded by an extremely large value of T [87], and the contributions to U can safely be dropped. Therefore, for points to be in agreement with the experimental observation, we require that the prediction of the S and the T parameter are within the 2σ ellipse, corresponding to $\chi^2 = 5.99$ for two degrees of freedom.

	Decrease $c_{h_1 b\bar{b}}$	No decrease $c_{h_1 t\bar{t}}$	No enhancement $c_{h_1 \tau\bar{\tau}}$
type I	✓ $\left(\frac{R_{12}}{s_\beta}\right)$	✗ $\left(\frac{R_{12}}{s_\beta}\right)$	✓ $\left(\frac{R_{12}}{s_\beta}\right)$
type II	✓ $\left(\frac{R_{11}}{c_\beta}\right)$	✓ $\left(\frac{R_{12}}{s_\beta}\right)$	✓ $\left(\frac{R_{11}}{c_\beta}\right)$
lepton-specific	✓ $\left(\frac{R_{12}}{s_\beta}\right)$	✗ $\left(\frac{R_{12}}{s_\beta}\right)$	✗ $\left(\frac{R_{11}}{c_\beta}\right)$
flipped	✓ $\left(\frac{R_{11}}{c_\beta}\right)$	✓ $\left(\frac{R_{12}}{s_\beta}\right)$	✗ $\left(\frac{R_{12}}{s_\beta}\right)$

Table 4. Conditions that have to be satisfied to accommodate the LEP and CMS excesses simultaneously with a light $\mathcal{CP}$-even scalar h_1 with dominant singlet component. In brackets we state the relevant coupling coefficients $c_{h_1 f\bar{f}}$ for the conditions for each type.

4 Experimental excesses

The main purpose of our analysis is to find a model that fits the two experimental excesses in the Higgs boson searches at CMS and LEP. As experimental input for the signal strengths we use the values

$$\mu_{\text{LEP}} = 0.117 \pm 0.057 \quad \text{and} \quad \mu_{\text{CMS}} = 0.6 \pm 0.2 , \tag{4.1}$$

as quoted in Refs. [5, 64] and [7, 88].

We evaluate the signal strengths for the excesses in the narrow width approximation. For the LEP excess this is given by,

$$\mu_{\text{LEP}} = \frac{\sigma_{\text{N2HDM}}(e^+ e^- \to Z h_1)}{\sigma_{\text{SM}}(e^+ e^- \to ZH)} \cdot \frac{\text{BR}_{\text{N2HDM}}(h_1 \to b\bar{b})}{\text{BR}_{\text{SM}}(H \to b\bar{b})} = |c_{h_1 VV}|^2 \frac{\text{BR}_{\text{N2HDM}}(h_1 \to b\bar{b})}{\text{BR}_{\text{SM}}(H \to b\bar{b})} , \tag{4.2}$$

where we assume that the cross section ratio can be expressed via the effective coupling of h_1 to vector bosons normalized to the SM prediction, which is provided by `N2HDECAY`, as is the branching ratio of h_1 to two photons. For the CMS signal strength one finds,

$$\mu_{\text{CMS}} = \frac{\sigma_{\text{N2HDM}}(gg \to h_1)}{\sigma_{\text{SM}}(gg \to H))} \cdot \frac{\text{BR}_{\text{N2HDM}}(h_1 \to \gamma\gamma)}{\text{BR}_{\text{SM}}(H \to \gamma\gamma)} = |c_{h_1 t\bar{t}}|^2 \frac{\text{BR}_{\text{N2HDM}}(h_1 \to \gamma\gamma)}{\text{BR}_{\text{SM}}(H \to \gamma\gamma)} . \tag{4.3}$$

The SM predictions for the branching ratios and the cross section via ggF can be found in Ref. [89]. We checked that the approximation of the cross section ratio in Eq. (4.3) with $|c_{h_1 t\bar{t}}|^2$ is accurate to the percent-level by comparing with the result for μ_{CMS} evaluated with the ggF cross section provided by `ScannerS`. Both approaches give equivalent results considering the experimental uncertainty in μ_{CMS}.

As can be seen from Eqs. (4.1) - (4.3), the CMS excess points towards the existence of a scalar with a SM-like production rate, whereas the LEP excess demands that the

scalar should have a squared coupling to massive vector bosons of ~ 0.1 times that of the SM Higgs boson of the same mass. This suppression of the coupling coefficient c_{h_1VV} is naturally fulfilled for a singlet-like state, that acquires its interaction to SM particles via a considerable mixing with the SM-like Higgs boson, thus motivating the explanation of the LEP excess with the real singlet of the N2HDM. For the CMS excess, on the other hand, it appears to be difficult at first sight to accommodate the large signal strength, because one expects a suppression of the loop-induced coupling to photons of the same order as the one of c_{h_1VV}, since in the SM the Higgs-boson decay to photons is dominated by the W boson loop. However, it turns out that it is possible to overcompensate the suppression of the loop-induced coupling to photons by decreasing the total width of the singlet-like scalar, leading to an enhancement of the branching ratio of the new scalar to the $\gamma\gamma$ final state. In principle, the branching ratio to diphotons can be further increased w.r.t. the SM by contributions stemming from diagrams with the charged Higgs boson in the loop. (In our scans, however, these contributions are of minor significance due to the high lower limit on the charged Higgs mass of 650 GeV from $\mathrm{BR}(B_s \to X_s\gamma)$ constraints.) The different types of N2HDM behave differently in this regard, based on how the doublet fields are coupled to the quarks and leptons. We summarize the general idea in Tab. 4 and argue that only the type II and type IV (flipped) N2HDM can accommodate both excesses simultaneously using a dominantly singlet-like scalar h_1 at ~ 96 GeV.

The first condition is that the coupling of h_1 to b-quarks has to be suppressed to enhance the decay rate to $\gamma\gamma$, as the total decay width at this mass is still dominated by the decay to $b\bar{b}$. At the same time one can not decrease the coupling to t-quarks too much, because the decay width to photons strongly depends on the top quark loop contribution (interfering constructively with the charged Higgs contribution). Moreover, the ggF production cross section is dominated at leading order by the diagram with t-quarks in the loop. Thus, a decreased coupling of h_1 to t-quarks implies a lower production cross section at the LHC. As one can deduce from Tab. 4, in type I and the lepton-specific N2HDM, the coupling coefficients are the same for up- and down-type quarks. Thus, it is impossible to satisfy both of the above criteria simultaneously in these models. Consequently, they fail to accommodate both the CMS and the LEP excesses.

One could of course go to the 2HDM-limit of the N2HDM by taking the singlet scalar to be decoupled, and reproduce the results observed previously in Refs. [12, 13], in which both excesses are accommodated placing the second $\mathcal{CP}$-even Higgs boson in the corresponding mass range. In the limit of the type I 2HDM, the parameter space favorable for the two excesses would correspond to very small values of coupling of the 96 GeV state to up-type quarks, because the dominant component of the scalar comes

from the down-type doublet field. This implies that the ggF production mode no longer dominates the total production cross section and the excesses can only be explained by considering the contributions from other modes of production like vector boson fusion and associated production with vector bosons etc. The results for the lepton-specific 2HDM follow closely the ones for type I because of similar coupling structures in the two models. In the CMS analysis [7], however, the excess appears clearly in the ggF production mode. Consequently, we discard these two versions of the N2HDM, as they cannot provide a sufficiently large ggF cross section, while yielding an adequate decay rate to $\gamma\gamma$ simultaneously.

Having discarded the type I and type III scenario, we now concentrate on the remaining two possibilities. In type II and the flipped type IV scenario, each of the doublet fields Φ_1 and Φ_2 couple to either up- or down-type quarks, and it is possible to control the size of the coupling coefficients $c_{h_i t\bar{t}}$ and $c_{h_i b\bar{b}}$ independently. Since the singlet-like scalar acquires its couplings to fermions through the mixing with the doublet fields, this effectively leads to one more degree of freedom to adjust its couplings independently for up- and down-type quarks. From the dependence of the mixing matrix elements R_{11} and R_{12} on the mixings angles α_i, as stated in Eq. (2.5), one can deduce that the relevant parameter in this case is α_1. For $|\alpha_1| \to \pi/2$ the up-type doublet component of h_1 is large and the down-type doublet component goes to zero. Thus, large values of α_1 will correspond to an enhancement of the branching ratio to photons, because the dominant decay width to b-quarks, and therefore the total width of h_1, is suppressed.

A third condition, although not as significant as the other two, is related to the coupling of h_1 to leptons. If it is increased, the decay to a pair of τ-leptons will be enhanced. Similar to the decay to b-quarks, it will compete with the diphoton decay and can suppress the signal strength needed for the CMS excess. The τ-Yukawa coupling is not as large as the b-Yukawa coupling, so this condition is not as important as the other two. Still, as we will see in our numerical evaluation, it is the reason why it is easier to fit the CMS excess in the type II model compared to the flipped scenario. In the latter the coupling coefficient to leptons is equal to the one to up-type quarks. Thus, in the region where the diphoton decay width is large, also decay width to τ-pairs is large, and both channels will compete. In the type II scenario, on the other hand, the coupling to leptons is equal to the coupling to down-type quarks, meaning that in the relevant parameter region both the decay to b-quarks and the decay to τ-leptons are suppressed.

In our scans we indicate the "best-fit point" referring to the point with the smallest

χ^2 defined by

$$\chi^2_{\mathrm{CMS-LEP}} = \frac{(\mu_{\mathrm{LEP}} - 0.117)^2}{0.057^2} + \frac{(\mu_{\mathrm{CMS}} - 0.6)^2}{0.2^2} \,, \tag{4.4}$$

quantifying the quadratic deviation w.r.t. the measured values, assuming that there is no correlation between the signal strengths of the two excesses. In principle, we could have combined the χ^2 obtained from `HiggsSignals` regarding the SM-like Higgs boson observables with the χ^2 defined above regarding the LEP and the CMS excesses. In that case, however, the total χ^2 would be strongly dominated by the SM-like Higgs boson contribution from `HiggsSignals` due to the sheer amount of signal strength observables implemented. Consequently, we refrain from performing such a combined χ^2 analysis.

ATLAS limits

ATLAS pubished first Run II results in the $\gamma\gamma$ searches below $125\,\mathrm{GeV}$ with $80\,\mathrm{fb}^{-1}$ [9]. No significant excess above the SM expectation was observed in the mass range between 65 and 110 GeV. However, the limit on cross section times branching ratio obtained in the diphoton final state by ATLAS is substantially weaker than the corresponding upper limit obtained by CMS at ~ 96 GeV. It does not touch the $1\,\sigma$ ranges of μ_{CMS}. Interestingly, the ATLAS result shows a little "shoulder" (upward "bump") around 96 GeV. This was illustrated and discussed in Fig. 1 of Ref. [10].

5 Results

In the following we will present our analyses in the type II and type IV scenario. The scalar mass eigenstate with dominant singlet-component will be responsible for accommodating the LEP and the CMS excesses at ~ 95-98 GeV. As already mentioned above, we performed a scan over the relevant parameters using the public code `ScannerS`. We give the ranges of the free parameters for each type in the corresponding subsection. We will make use of the possibility to set additional constraints on the singlet admixture of each $\mathcal{CP}$-even scalar particle, which is provided by `ScannerS`. Additional constraints on the mixing angles α_i, as will be explained in the following, were implemented by us within the appropriate routines to exclude irrelevant parameter space.

In our plots we will show the benchmark points that pass all the theoretical and experimental constraints described in Sect. 3, if not said otherwise. We will provide details on the best-fit points for both types of the N2HDM and explain relevant differences regarding the contributions to the excesses at LEP and CMS.

Similar scans have been performed also for the N2HDM type I and III (lepton specific). We confirmed the negative result expected from the arguments given in

Sect. 4. Consequently, we do not show any of these results here, but concentrate on the two models that indeed can describe the CMS and LEP excesses.

To enforce that the lightest scalar has the dominant singlet admixture, we impose

$$65\% \leq \Sigma_{h_1} \leq 90\% \,, \tag{5.1}$$

while for the SM-like Higgs boson we impose a lower limit on the singlet admixture of

$$\Sigma_{h_2} \geq 10\% \,. \tag{5.2}$$

This assures that there is at least some doublet component in h_1 in each scan point, which is necessary to fit the excesses. We have checked explicitly that this bound has no impact on the parameter space that have $\chi^2_{\mathrm{CMS-LEP}} \leq 2.30$ (i.e. the $1\,\sigma$ range, see the discussion of Fig. 10 below). The conditions on the singlet admixture of the mass eigenstates can trivially be translated into bounds on the mixing angles α_i. Taking into account that we want to increase the up-type component of h_1 compared to its down-type component, one can deduce from the definition of the mixing matrix in Eq. (2.5) that $\alpha_1 \to \pm\pi/2$ is a necessary condition. In this limit the coupling coefficients of the SM-like Higgs boson h_2 to quarks can be approximated by

$$c_{h_2 t\bar{t}} \sim \mp \frac{s_{\alpha_2} s_{\alpha_3}}{s_\beta} \quad \text{and} \quad c_{h_2 b\bar{b}} \sim \mp \frac{c_{\alpha_3}}{c_\beta} \,. \tag{5.3}$$

Consequently, if α_2 and α_3 would have opposite signs, one would be in the wrong-sign Yukawa coupling regime. In this regime it is harder to accommodate the SM-like Higgs boson properties, especially for low values of $\tan\beta$. Also the possible singlet-component of h_2 is more limited [37]. To avoid entering the wrong-sign Yukawa coupling regime, we therefore impose additionally

$$\alpha_2 \cdot \alpha_3 > 0 \,. \tag{5.4}$$

5.1 Type II

Following the discussion about the various experimental and theoretical constrains we chose to scan the following range of input parameters:

$$95 \text{ GeV} \leq m_{h_1} \leq 98 \text{ GeV} \,, \quad m_{h_2} = 125.09 \text{ GeV} \,, \quad 400 \text{ GeV} \leq m_{h_3} \leq 1000 \text{ GeV} \,,$$
$$400 \text{ GeV} \leq m_A \leq 1000 \text{ GeV} \,, \quad 650 \text{ GeV} \leq M_{H^\pm} \leq 1000 \text{ GeV} \,,$$
$$0.5 \leq \tan\beta \leq 4 \,, \quad 0 \leq m_{12}^2 \leq 10^6 \text{ GeV}^2 \,, \quad 100 \text{ GeV} \leq v_S \leq 1500 \text{ GeV} \,. \tag{5.5}$$
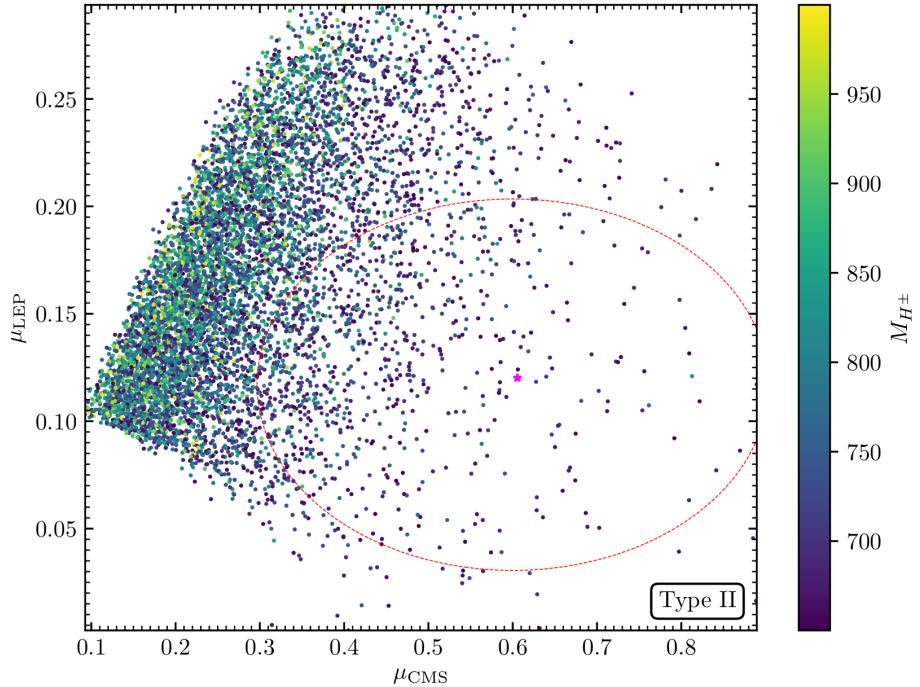
Figure 1. Type II: the signal strengths μ_{CMS} and μ_{LEP} are shown for each scan point respecting the experimental and theoretical constrains. The $1\,\sigma$-region of both excesses is shown by the red ellipse. The colors show the mass of the charged Higgs. The magenta star is the best-fit point. The lowest (highest) value of $M_{H^\pm}$ inside the $1\,\sigma$ ellipse is 650.03 (964.71) GeV.

We show the result of our scan in Figs. 1-3 in the plane of the signal strengths μ_{LEP} and μ_{CMS} for each scan point, where the best-fit point w.r.t. the two excesses is marked by a magenta star. It should be kept in mind that the density of points has no physical meaning and is a pure artifact of the "flat prior" in our parameter scan. The red dashed line corresponds to the $1\,\sigma$ ellipse, i.e., to $\chi^2_{\text{CMS}-\text{LEP}} = 2.30$ for two degrees of freedom, with $\chi^2_{\text{CMS}-\text{LEP}}$ defined in Eq. (4.4). The colors of the points indicate the value of the charged Higgs mass in Fig. 1 and the reduced χ^2 (see Eq. (3.5)) from the test of the SM-like Higgs-boson properties with `HiggsSignals` in Fig. 2. One sees that various points fit both excesses simultaneously while also accommodating the properties of the SM-like Higgs boson at 125 GeV. From Fig. 1 we can conclude that lower values for $M_{H^\pm}$ are preferred to fit the diphoton excess. We emphasize that the dependence of the branching ratio of h_1 to diphotons, and therefore of μ_{CMS}, on $M_{H^\pm}$ is due to the positive correlation between $M_{H^\pm}$ and the total decay width of h_1. The additional contributions to the diphoton decay width of diagrams with the charged Higgs boson in the loop has a minor dependence on $M_{H^\pm}$ for $M_{H^\pm} > 650$ GeV. When $M_{H^\pm}$ becomes larger the constraints from the oblique parameters induce also larger
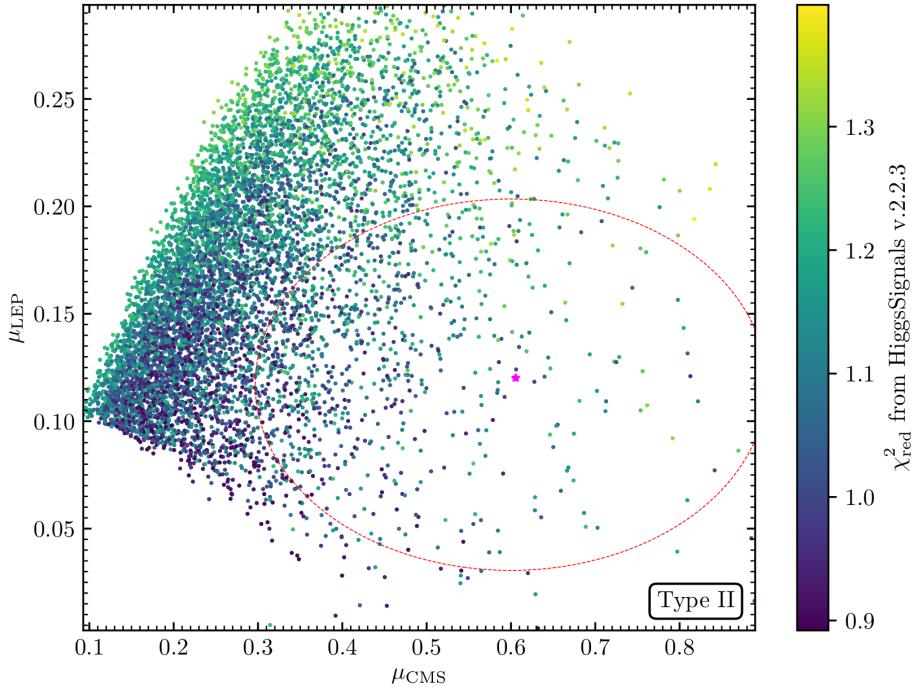
Figure 2. Type II: as in Fig. 1, but here the colors indicate the $\chi^2_{\rm red}$ from HiggsSignals. The best-fit point (magenta) has $\chi^2_{\rm red} = 1.237$ with 101 observations considered. The lowest (highest) value of $\chi^2_{\rm red}$ inside the $1\,\sigma$ ellipse is 0.9052 (1.3304).

masses of the heavy Higgs m_{h_3} and the $\mathcal{CP}$-odd Higgs m_A. These masses are correlated to the mixing angles in the scalar sector via the tree-level perturbative unitarity and global minimum conditions. Concerning a large suppression of the total decay width of h_1, and thus an enhancement of $\mathrm{BR}_{h_1}^{\gamma\gamma}$, it turns out to be more difficult to achieve for larger m_{h_3}, $M_{H^\pm}$ and M_A. Finally, we show in Fig. 3 a plot with the colors indicating the value of $\tan\beta$ in each point. An overall tendency can be observed that values of about $\tan\beta \sim 1$ are preferred in our scan. However, we find points covering the whole $\tan\beta$-range used in our scan within the $1\,\sigma$ ellipse of the excesses.

The preferred low values of the charged Higgs mass and $\tan\beta$ give rise to the fact that the scenario presented here will be in reach of direct searches for charged Higgs bosons at the LHC [41] (see the discussion in Sect. 5.3.1). Already now, parts of the parameter space scanned here are excluded by direct searches. This is illustrated in Fig. 4a, where we show points allowed by `HiggsBounds` in green, and the excluded points in red. For values of $\tan\beta < 1$ direct searches are very constraining. The experimental analysis responsible for this excluded region is the search for charged Higgs bosons produced in association with a t- and a b-quark, and the subsequent
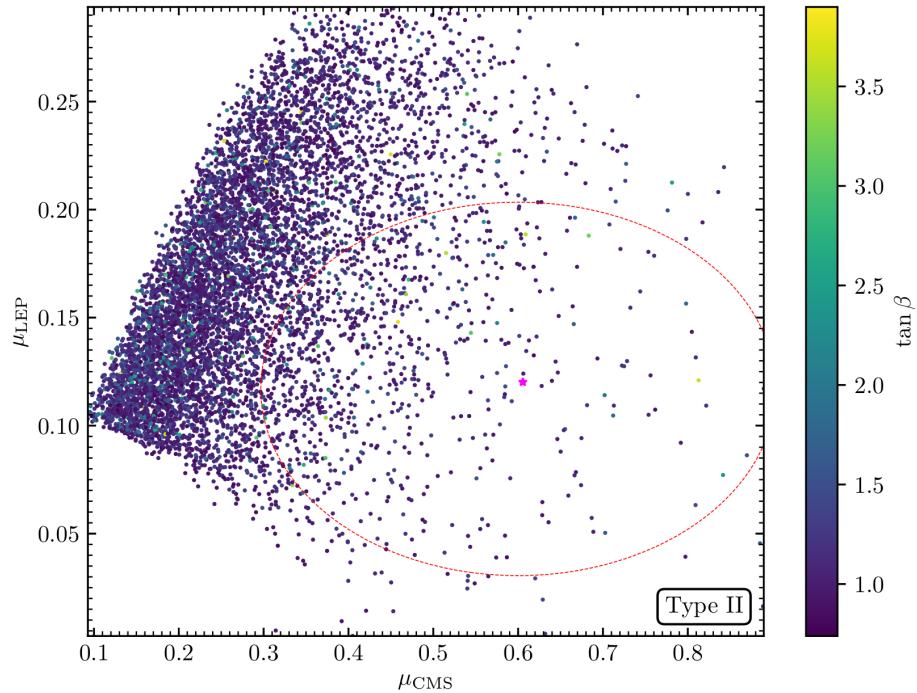
Figure 3. Type II: as in Fig. 1, but here the colors indicate the value of $\tan\beta$. The lowest (highest) value of $\tan\beta$ inside the 1σ ellipse is 0.7970 (3.748).
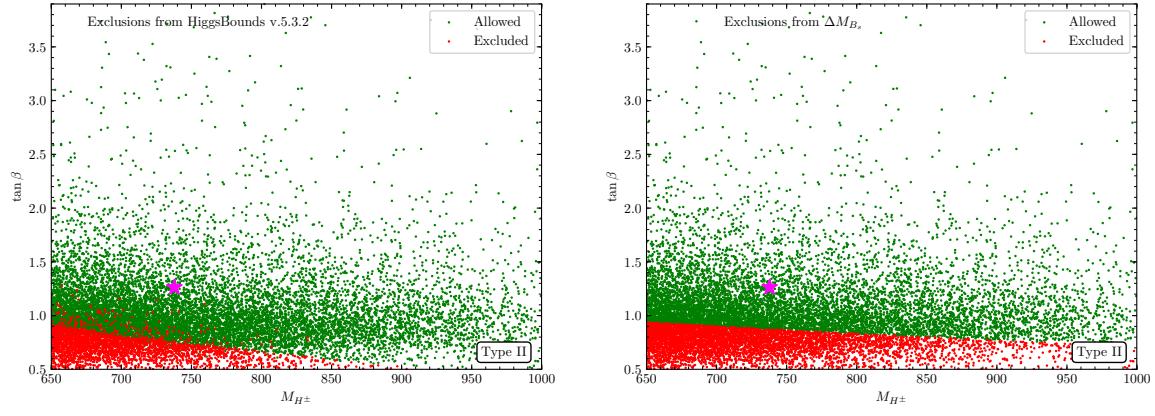

(a) Direct searches at colliders in type II.

(b) Flavor physics in type II.

Figure 4. Allowed (*green*) and excluded (*red*) points considering direct searches (*left*) and flavor physics (*right*) in the $M_{H^\pm}$-$\tan\beta$ plane. The magenta star is the best-fit point.

decay of the charged Higgs boson to a *tb*-pair, performed by ATLAS [41]. Apart from that, flavor physics can provide very strict bounds in the $M_{H^\pm}$-$\tan\beta$ plane (see the discussion in Sect. 3.4). We show the excluded regions in our scan in Fig. 4b. We see that in the region of lower values of the charged Higgs-boson mass, where the excesses are reproduced most "easily", bounds from flavor physics are as good as the direct searches for additional Higgs bosons in the low $\tan\beta$ region. Values of $\tan\beta < 0.7$ are ruled out for the whole range of $M_{H^\pm}$.

In Tab. 5 we show the values of the free parameters and the relevant branching ratios of the singlet-like scaler h_1, the SM-like Higgs boson h_2 as well as all other (heavier) Higgs bosons of the model for the best-fit point of our scan, which is highlighted with a magenta star in Figs. 1-4b. Remarkably, the branching ratio for the singlet-like scalar to photons is larger than the one of the SM-like Higgs boson. As explained in the beginning of Sect. 5 this is achieved by a value of $\alpha_1 \sim \pi/2$, which suppresses the decay to b-quarks and τ-leptons, without decreasing the coupling to t-quarks. The most important BRs for the heavy Higgs bosons are those to the heaviest quarks, $h_3 \to t\bar{t}$, $A \to t\bar{t}$ and $H^\pm \to tb$, offering interesting prospects for future searches, as will be briefly discussed in Sect. 5.3. Constraints from the oblique parameters lead to a $\mathcal{CP}$-odd Higgs boson mass m_A close to the mass of the charged Higgs boson. We stress, however, that this is not the only possibility to fulfill the constraints from the oblique parameters. The alternative possibility that $m_{h_3} \sim M_{H^\pm}$ occurs as often as $m_A \sim M_{H^\pm}$ in our scan. The value of $\tan\beta$ is close to one, meaning that the benchmark point shown here might be in range of future improved constraints both from direct searches at colliders as well as from flavor physics. More optimistically speaking, deviations from the SM predictions are expected in those observables if our explanation of the LEP and CMS excesses are implemented by nature. We will discuss in Sect. 5.3 the prospects of detecting deviations from the SM-prediction, that accompany our explanation of the LEP and the CMS excess, at future colliders.

5.2 Type IV (flipped)

In the type IV (flipped) scenario the couplings of the scalars to quarks are unchanged with respect to the type II scenario. The coupling to leptons, however, is equal to the coupling to the up-type quarks, instead of being equal to the coupling to down-type quarks, as it is in the type II scenario. This means that while the parameter space that can fit the LEP and the CMS excesses will be very similar to the one in the type II analysis, the non-suppression of the decay width of h_1 to τ-leptons will have to be compensated. Apart from that, constrains especially from the SM-like Higgs boson measurements and from direct searches will be different (see also Sect. 5.3). For the scan in the type IV scenario we choose the same range of parameters as in the type II

m_{h_1}	m_{h_2}	m_{h_3}	m_A	$M_{H^\pm}$		
96.5263	125.09	535.86	712.578	737.829		

$\tan\beta$	α_1	α_2	α_3	m_{12}^2	v_S	
1.26287	1.26878	-1.08484	-1.24108	80644.3	272.72	

$\mathrm{BR}_{h_1}^{bb}$	$\mathrm{BR}_{h_1}^{gg}$	$\mathrm{BR}_{h_1}^{cc}$	$\mathrm{BR}_{h_1}^{\tau\tau}$	$\mathrm{BR}_{h_1}^{\gamma\gamma}$	$\mathrm{BR}_{h_1}^{WW}$	$\mathrm{BR}_{h_1}^{ZZ}$
0.5048	0.2682	0.1577	0.0509	$2.582 \cdot 10^{-3}$	0.0137	$1.753 \cdot 10^{-3}$

$\mathrm{BR}_{h_2}^{bb}$	$\mathrm{BR}_{h_2}^{gg}$	$\mathrm{BR}_{h_2}^{cc}$	$\mathrm{BR}_{h_2}^{\tau\tau}$	$\mathrm{BR}_{h_2}^{\gamma\gamma}$	$\mathrm{BR}_{h_2}^{WW}$	$\mathrm{BR}_{h_2}^{ZZ}$
0.5916	0.0771	0.0288	0.0636	$2.153 \cdot 10^{-3}$	0.2087	0.0261

$\mathrm{BR}_{h_3}^{tt}$	$\mathrm{BR}_{h_3}^{gg}$	$\mathrm{BR}_{h_3}^{h_1 h_1}$	$\mathrm{BR}_{h_3}^{h_1 h_2}$	$\mathrm{BR}_{h_3}^{h_2 h_2}$	$\mathrm{BR}_{h_3}^{WW}$	$\mathrm{BR}_{h_3}^{ZZ}$
0.8788	$2.537 \cdot 10^{-3}$	0.0241	0.0510	$3.181 \cdot 10^{-3}$	0.0261	0.0125

BR_A^{tt}	BR_A^{gg}	$\mathrm{BR}_A^{Zh_1}$	$\mathrm{BR}_A^{Zh_3}$	BR_A^{bb}		
0.6987	$1.771 \cdot 10^{-3}$	0.1008	0.1981	$5.36 \cdot 10^{-4}$		

$\mathrm{BR}_{H^\pm}^{tb}$	$\mathrm{BR}_{H^\pm}^{Wh_3}$	$\mathrm{BR}_{H^\pm}^{Wh_1}$				
0.6000	0.3004	0.0984				

Table 5. Parameters of the best-fit point and branching ratios of the scalars in the type II scenario. Dimensionful parameters are given in GeV and the angles are given in radian.

scenario, shown in Eq. (5.5). As explained in the beginning of Sect. 5 we further impose Eq. (5.4).

We show the results of our scan in the flipped scenario in Figs. 5-7. Again, the color code quantifies the charged Higgs-boson mass in Fig. 5, the reduced χ^2 from `HiggsSignals` in Fig. 6, and the value of $\tan\beta$ in Fig. 7. As was the case in the type II scenario, a large number of points fit both the LEP and the CMS excesses simultaneously while being in agreement with the measurements of the SM-like Higgs boson properties. We again observe that the points that fit both excesses prefer low values of $M_{H^\pm}$ for the same reasons as in the type II scenario (see Sect. 5.1). Various points inside the $1\,\sigma$ ellipse have additionally a $\chi^2_{\rm red}$ from `HiggsSignals` below one, indicating the signal strength predictions for the SM-like Higgs boson on average are within the $1\,\sigma$-uncertainties of each measurement. Similar to the type II analysis a clear preference of small $\tan\beta$-values is visible, also for the points outside the $1\,\sigma$ ellipse.

The exclusion boundaries from direct searches and from flavor physics are practically the same as the ones we found in the type II scenario. We show in Fig. 8a the allowed and excluded points of our scan considering the collider searches in the $\tan\beta$-

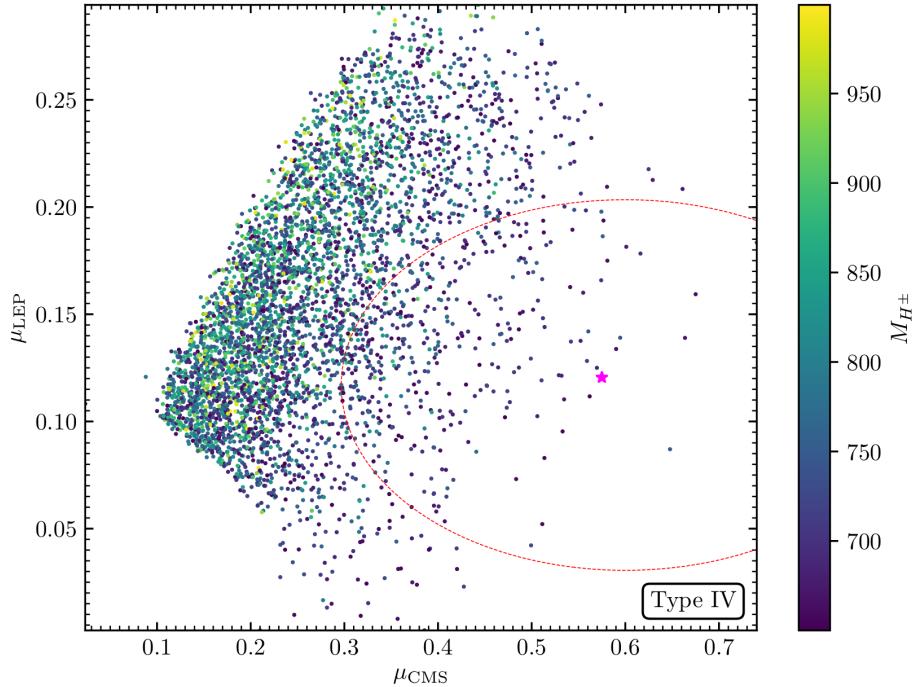**Figure 5**. Type IV: the signal strengths μ_{CMS} and μ_{LEP} for each scan point respecting the experimental and theoretical constrains. The 1σ-region of both excesses is shown by the red ellipse. The colors show the mass of the charged Higgs. The magenta star indicates the best-fit point. The lowest (highest) value of $M_{H^\pm}$ inside the 1σ ellipse is 650.01 (931.85) GeV.

$M_{H^\pm}$ plane. The most sensitive direct search is, as in type II, the production of $H^\pm$ in association with a *tb*-pair, and subsequent decay of $H^\pm$ to a *tb*-pair. For values of $\tan\beta < 1$, points with a charged Higgs mass up to 900 GeV can be excluded. In Fig. 8b we show the excluded and allowed points regarding constraints derived from the prediction to the meson mass difference ΔM_{B_s}. This limit is unchanged with respect to the one from the type II scenario, because of the similar quark Yukawa sectors in the two cases. ΔM_{B_s} constraint is the dominant one regarding flavor observables for the range of $M_{H^\pm}$ and $\tan\beta$ scanned here, assuming that the exclusions from $\mathrm{BR}(B_s \to \mu^+\mu^-)$ constraints in the 2HDM do not change by more than 20% due to the presence of the additional real singlet in the N2HDM [40].

The details of our best-fit point of the scan in the N2HDM type IV, indicated with the magenta star in Figs. 5-8b, are listed in Tab. 6. The value of the charged Higgs boson mass is just on the lower end of the scanned range. Comparing to the best-fit point of our scan in the N2HDM type II, shown in Tab. 5, we observe that the values for $\tan\beta$ and the mixing angles in the $\mathcal{CP}$-even scalar sector α_i are very similar. This is due to the fact that the effective coefficients of the couplings of the scalars to
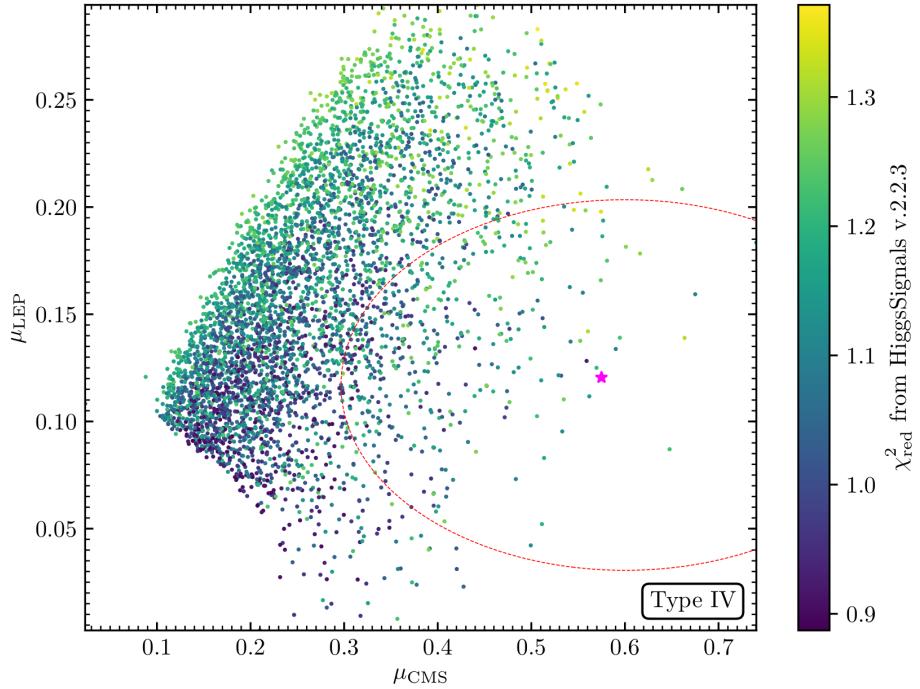
Figure 6. Type IV: as in Fig. 5, but here the colors indicate the $\chi^2_{\rm red}$ from HiggsSignals. The best-fit point (magenta) has $\chi^2_{\rm red} = 1.11286$ with 101 observations considered. The lowest (highest) value of $\chi^2_{\rm red}$ within the $1\,\sigma$ ellipse is 0.9073 (1.3435).

quarks are the same. Also the decays of the heavier Higgs bosons are similar to the type II best-fit point. The striking difference between the best-fit points in both types is that, even though the suppression of the branching ratio of h_1 to b-quarks is larger in type IV, the branching ratio to photons remains smaller. As already discussed in Sect. 4, in the parameter region, in which the excesses can be accommodated, there is an enhancement of the decay width to τ-leptons: the value for $\mathrm{BR}^{\tau\tau}_{h_1}$ in Tab. 6 is roughly five times larger than the one in Tab. 5.

This circumstance is not a particular feature of the best-fit point, but a general difference between type II and type IV. To illustrate this, we show in Fig. 9 the branching ratio of h_1 to photons (top) and to τ-leptons (bottom) for type II (left) and type IV (right) as a function of the absolute value of the ratio of the effective coupling coefficients $c_{h_1 b\bar{b}}$ and $c_{h_1 t\bar{t}}$. The blue and red points are the ones lying inside and outside the $1\,\sigma$ ellipse regarding $\chi^2_{\rm CMS-LEP}$, respectively. When $|c_{h_1 b\bar{b}}/c_{h_1 t\bar{t}}|$ is small, the branching ratios to photons receives an enhancement and it is possible to fit the CMS excess. However, in type II the enhancement is larger than in type IV, because the branching ratio to τ-leptons scales with the same factor as $c_{h_1 b\bar{b}}$ in type II, but proportional to $c_{h_1 t\bar{t}}$ in type IV.
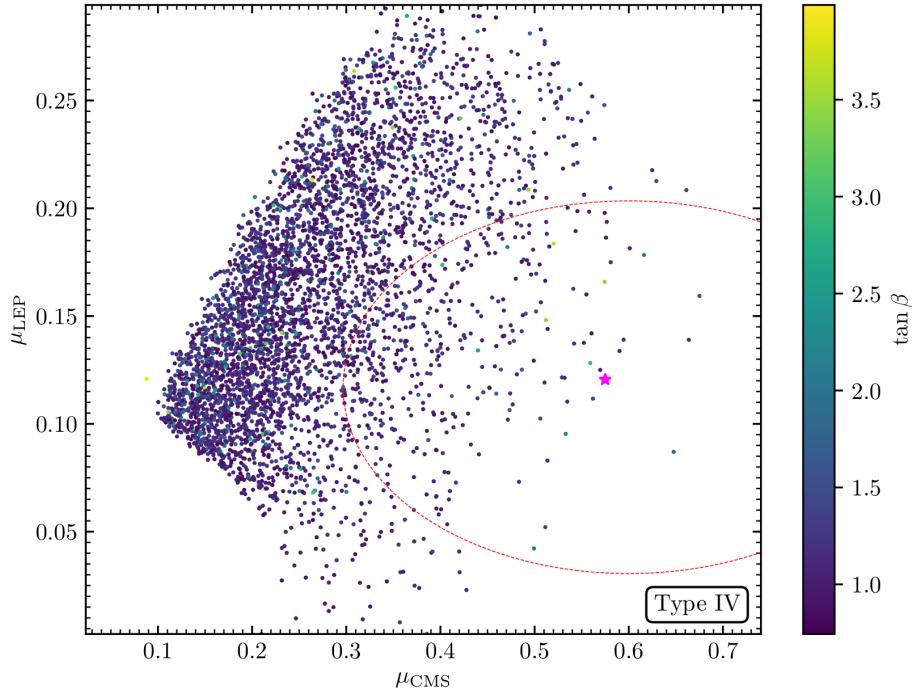
Figure 7. Type IV: as in Fig. 1, but here the colors indicate the value of $\tan\beta$. The lowest (highest) value of $\tan\beta$ within the $1\,\sigma$ ellipse is 0.7935 (3.592).

(a) Direct searches at colliders
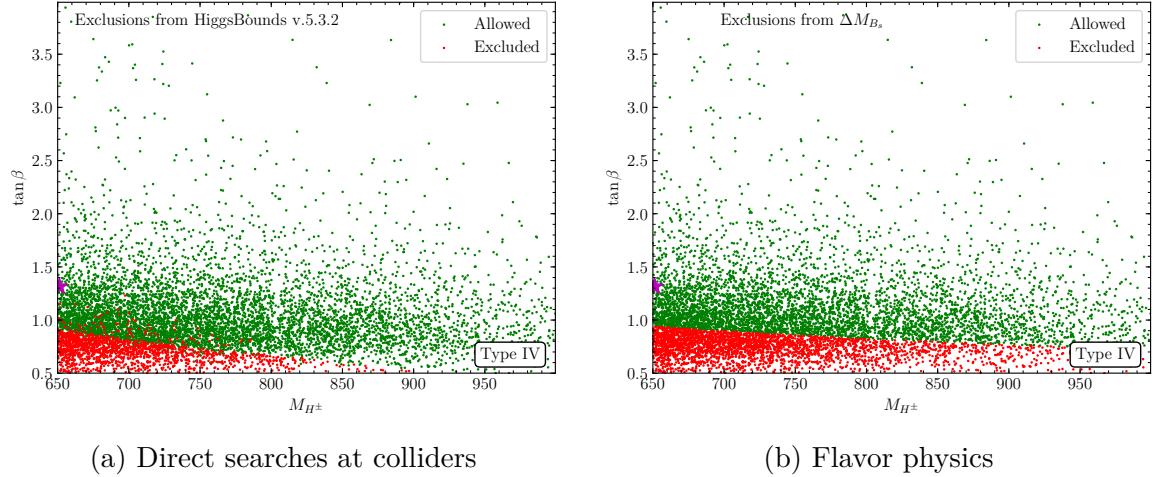
(b) Flavor physics

Figure 8. Allowed (*green*) and excluded (*red*) points considering direct searches (*left*) and flavor physics (*right*) in the $M_{H^\pm}$-$\tan\beta$ plane. The magenta star is the best-fit point.

m_{h_1}	m_{h_2}	m_{h_3}	m_A	$M_{H^\pm}$		
97.8128	125.09	485.998	651.502	651.26		

$\tan\beta$	α_1	α_2	α_3	m_{12}^2	v_S	
1.3147	1.27039	-1.02829	-1.32496	41034.1	647.886	

$\mathrm{BR}_{h_1}^{bb}$	$\mathrm{BR}_{h_1}^{gg}$	$\mathrm{BR}_{h_1}^{cc}$	$\mathrm{BR}_{h_1}^{\tau\tau}$	$\mathrm{BR}_{h_1}^{\gamma\gamma}$	$\mathrm{BR}_{h_1}^{WW}$	$\mathrm{BR}_{h_1}^{ZZ}$
0.4074	0.2071	0.1189	0.2483	$2.139 \cdot 10^{-3}$	0.0135	$1.579 \cdot 10^{-3}$

$\mathrm{BR}_{h_2}^{bb}$	$\mathrm{BR}_{h_2}^{gg}$	$\mathrm{BR}_{h_2}^{cc}$	$\mathrm{BR}_{h_2}^{\tau\tau}$	$\mathrm{BR}_{h_2}^{\gamma\gamma}$	$\mathrm{BR}_{h_2}^{WW}$	$\mathrm{BR}_{h_2}^{ZZ}$
0.5363	0.0939	0.0345	0.0758	$2.247 \cdot 10^{-3}$	0.2267	0.0284

$\mathrm{BR}_{h_3}^{tt}$	$\mathrm{BR}_{h_3}^{gg}$	$\mathrm{BR}_{h_3}^{h_1 h_1}$	$\mathrm{BR}_{h_3}^{h_1 h_2}$	$\mathrm{BR}_{h_3}^{h_2 h_2}$	$\mathrm{BR}_{h_3}^{WW}$	$\mathrm{BR}_{h_3}^{ZZ}$
0.8078	$2.707 \cdot 10^{-3}$	0.0124	$2.111 \cdot 10^{-3}$	0.0119	0.1085	0.0517

BR_{A}^{tt}	BR_{A}^{gg}	$\mathrm{BR}_{A}^{Zh_1}$	$\mathrm{BR}_{A}^{Zh_2}$	$\mathrm{BR}_{A}^{Zh_3}$	BR_{A}^{bb}	
0.7090	$1.940 \cdot 10^{-3}$	0.1007	$9.652 \cdot 10^{-3}$	0.1780	$6.49 \cdot 10^{-4}$	

$\mathrm{BR}_{H^\pm}^{tb}$	$\mathrm{BR}_{H^\pm}^{Wh_3}$	$\mathrm{BR}_{H^\pm}^{Wh_2}$	$\mathrm{BR}_{H^\pm}^{Wh_1}$			
0.6820	0.2046	$9.820 \cdot 10^{-3}$	0.1024			

Table 6. Parameters of the best-fit point and branching ratios of the scalars in the type IV scenario. Dimensionful parameters are given in GeV and the angles are given in radian.

In Fig. 10 we show the signal strengths for both excesses in the N2HDM type II (left) and type IV (right), with colors indicating the singlet component of h_1. Comparing both plots, it becomes apparent that the effect mentioned above results in a substantial suppression of μ_{CMS} in the type IV scenario. For similar values of the singlet component Σ_{h_1}, the type II scenario can reach larger μ_{CMS}, whereas the size of μ_{LEP} is very similar in both scenarios. Remarkably, the type II scenario can reach values of $\mu_{\mathrm{CMS}} \sim 1$, meaning that the signal strength prediction for μ_{CMS} is as big as the one of a hypothetical SM-like Higgs boson at the same mass, even though it is dominantly singlet-like. In the type IV scenario, on the other hand, there is no point above the upper $1\,\sigma$-limit of $\mu_{\mathrm{CMS}} = 0.8$. As one can anticipate form these plots, points with $\Sigma_{h_1} \geq 0.9$ are not expected in the $1\,\sigma$ ellipse. We have verified this by dedicated scans, i.e. it is confirmed that $\Sigma_{h_1} \leq 0.9$ does not have a relevant impact on the overall results of our analysis.
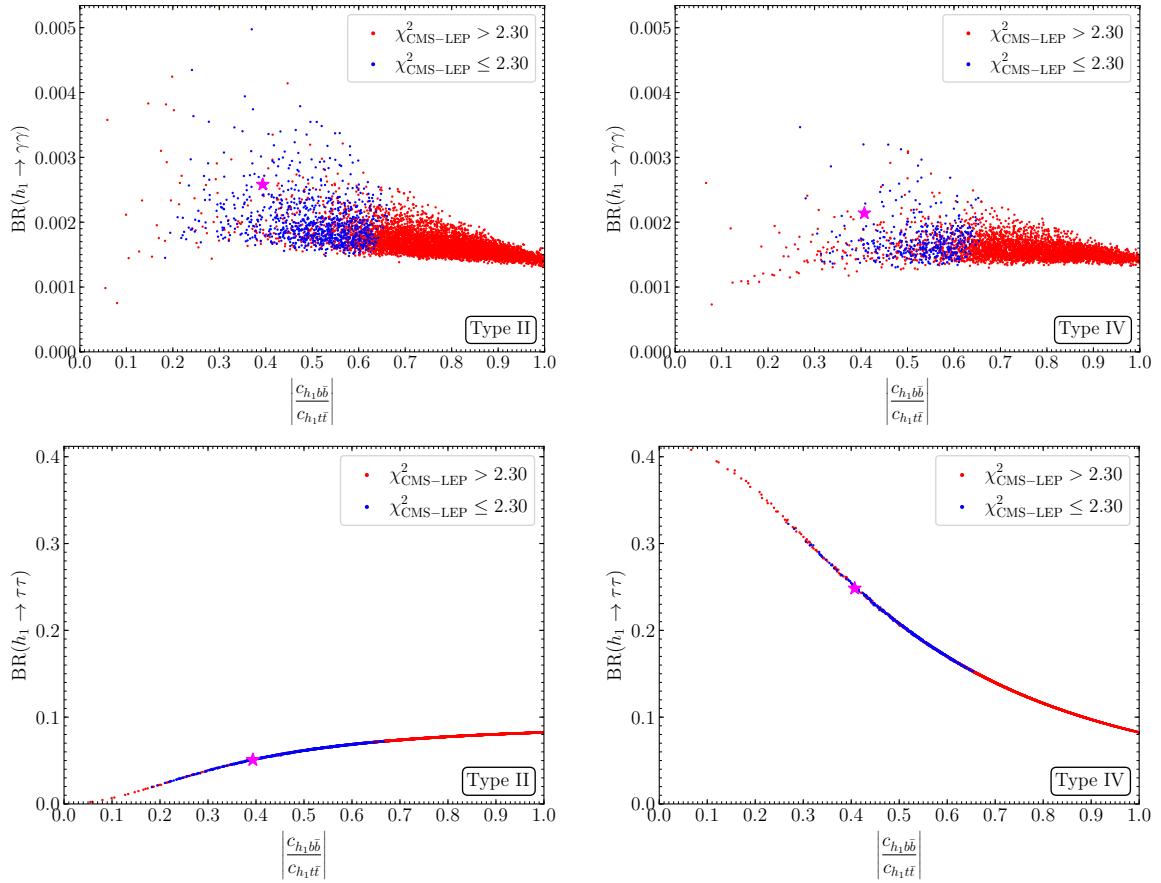
Figure 9. Branching fraction of h_1 to two photons (*upper row*) and to two τ-leptons (*lower row*) for each parameter point respecting the experimental and theoretical constrains in the type II (*left*) and the type IV scenario (*right*) as a function of the ratio of the coupling of h_1 to bottom and top quarks normalized to the SM prediction. The blue points have $\chi^2_{\text{CMS-LEP}} \leq 2.30$, while the red points have $\chi^2_{\text{CMS-LEP}} > 2.30$.

5.3 Future searches

A light singlet-like light scalar, as is present in the N2HDM, is very challenging to directly search for at the LHC, because of its suppressed couplings to all SM particles. That is why it might have escaped discovery so far except for some alluring hints two of which we have focussed on in this work. Indirect probes for such a particle are possible with precision measurements of the couplings of the 125 GeV Higgs state. We will discuss both possibilities as well as searches for heavy Higgs bosons in the following.

(a) Type II   (b) Type IV (flipped)
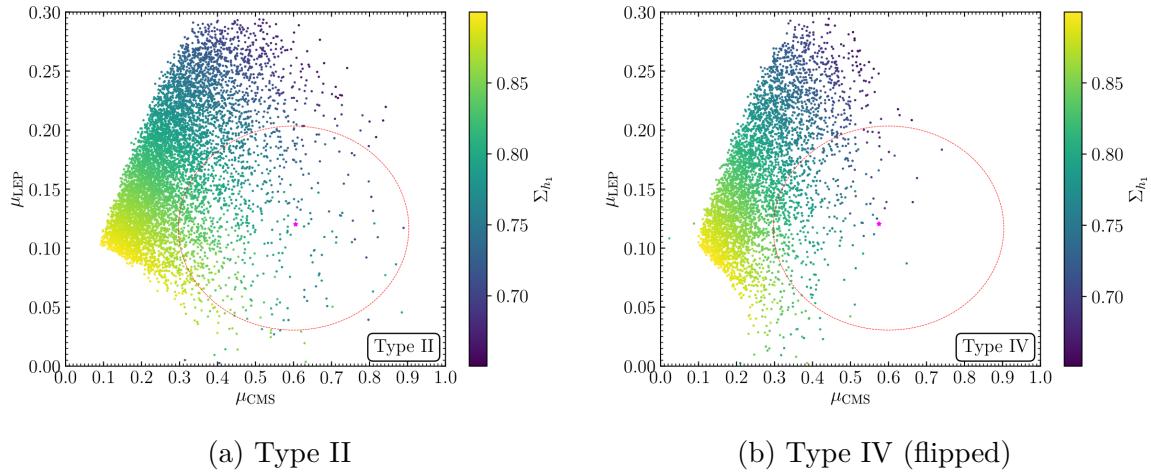
Figure 10. Shown are the signal strengths μ_{CMS} and μ_{LEP} for each parameter point respecting the experimental and theoretical constrains in the type II and the type IV scenario. The $1\,\sigma$-region of both excesses is shown by the red ellipse. The colors show the singlet component of h_1. The magenta star is the best-fit point.

5.3.1   Indirect searches

Currently, uncertainties on the measurement of the coupling strengths of the SM-like Higgs boson at the LHC are still large, i.e., at the $1\,\sigma$-level they are of the same order as the modifications of the couplings present in our analysis in the N2HDM [3, 90, 91]. In the future, once the complete $300\,\text{fb}^{-1}$ collected at the LHC are analyzed, the constraints on the couplings of the SM-like Higgs boson will benefit from the reduction of statistical uncertainties. Even tighter constraints are expected from the LHC after the high-luminosity upgrade (HL-LHC), when the planned amount of $3000\,\text{fb}^{-1}$ integrated luminosity will have been collected [92]. Finally, a future linear e^+e^- collider like the ILC could improve the precision measurements of the Higgs boson couplings even further [92, 93].[2] Firstly, a lepton collider has the advantage of massively reduced QCD background compared to a hadron collider like the LHC. Secondly, the cross section of the Higgs boson can be measured independently, and the total width (and therefore also the coupling modifiers) can be reconstructed without model assumptions.

Several studies have been performed to estimate the future constraints on the coupling modifiers of the SM-like Higgs boson at the LHC [92, 94–97] and the ILC [92, 98–103], assuming that no deviations from the SM predictions will be found. Here, we illustrate the capability of both experiments to either rule out or confirm the scenarios

---

[2]Similar results can be obtained for CLIC, FCC-ee and CEPC. We will focus on the ILC prospects here using the results of Ref. [93].

we presented in our paper. We compare our scan points to the expected precisions of the LHC and the ILC as they are reported in Refs. [102, 103], neglecting possible correlations of the coupling modifiers.

In Fig. 11 we plot the effective coupling coefficient of the SM-like Higgs boson h_2 to τ-leptons on the horizontal axis against the coupling coefficient to b-quarks (top) and to t-quarks (bottom) for both types. These points passed all the experimental and theoretical constraints, including the verification of SM-like Higgs boson properties in agreement with LHC results using `HiggsSignals`. In the top plot the blue points lie on a diagonal line, because in type II the coupling to leptons and to down-type quarks scale identically, while in the bottom plot the red points representing the type IV scenario lie on the diagonal, because there the lepton-coupling scales in the same way as the coupling to up-type quarks. The current measurements on the coupling modifiers by ATLAS [90] and CMS [91] are shown as black ellipses, although the corresponding uncertainties are still very large.

The magenta ellipse in each plot shows the expected precision of the measurement of the coupling coefficients at the $1\,\sigma$-level at the HL-LHC from Ref. [103]. The current uncertainties and the HL-LHC analysis are based on the coupling modifier, or κ-framework, in which the tree-level couplings of the SM-like Higgs boson to vector bosons, the top quark, the bottom quark, the τ and the μ lepton, and the three loop-induced couplings to $\gamma\gamma$, gg and $Z\gamma$ receive a factor κ_i quantifying potential modifications from the SM predictions. These modifiers are then constrained using a global fit to projected HL-LHC data assuming no deviation from the SM prediction will be found. The uncertainties found for the κ_i can directly be applied to the future precision of the coupling modifiers $c_{h_i\dots}$ we use in our paper. We use the uncertainties given under the assumptions that no decay of the SM-like Higgs boson to BSM particles is present, and that current systematic uncertainties will be reduced in addition to the reduction of statistical uncertainties due to the increased statistics.

The green and the orange ellipses show the corresponding expected uncertainties when the HL-LHC results are combined with projected data from the ILC after the 250 GeV phase and the 500 GeV phase, respectively, taken from Ref. [102]. Their analysis is based on a pure effective field theory calculation, supplemented by further assumptions to facilitate the combination with the HL-LHC projections in the κ-framework. In particular, in the effective field theory approach the vector boson couplings can be modified beyond a simple rescaling. This possibility was excluded by recasting the fit setting two parameters related to the couplings to the Z-boson and the W-boson to zero (for details we refer to Ref. [102]).

Remarkably, while current constraints on the SM-like Higgs-boson properties allow for large deviations of the couplings of up to 40%, the parameter space of our scans will
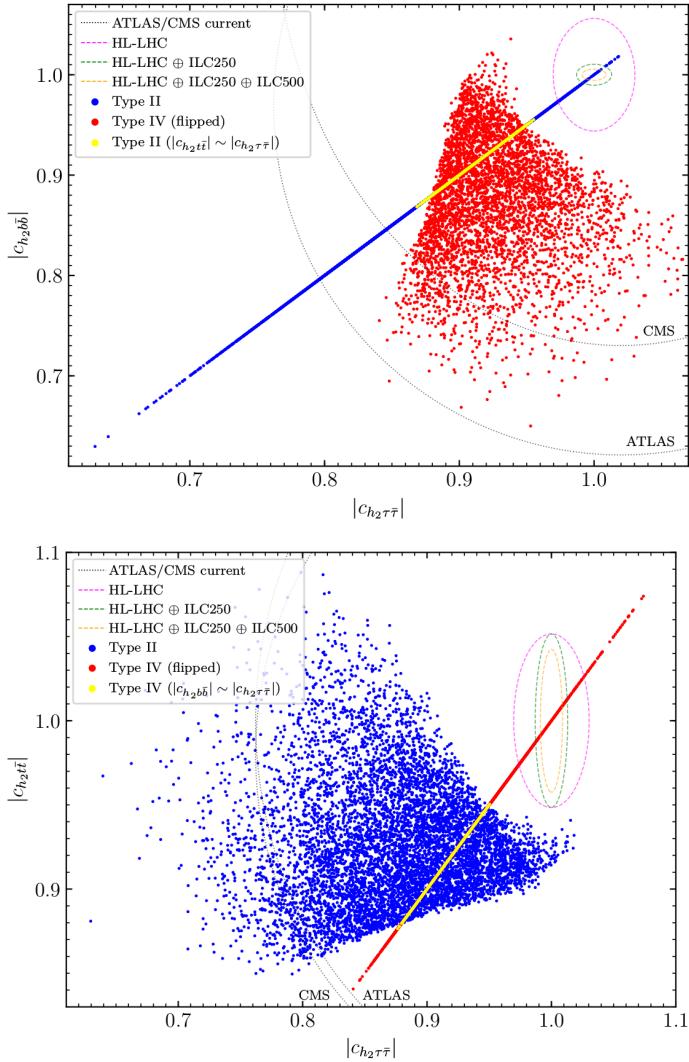
Figure 11. Scan points of our analysis in the type II (*blue*) and type IV (*red*) scenario in the $|c_{h_2\tau\bar\tau}|$-$|c_{h_2b\bar b}|$ plane (*top*) and the $|c_{h_2\tau\bar\tau}|$-$|c_{h_2t\bar t}|$ plane (*bottom*). In the upper plot we highlight in yellow the points of the type II scenario that overlap with points from the type IV scenario in the lower plot, i.e., points with $|c_{h_2t\bar t}| \sim |c_{h_2b\bar b}| \sim |c_{h_2\tau\bar\tau}|$. In the same way in the lower plot we highlight in yellow the points of the type IV scenario that overlap with points from the type II scenario in the upper plot. The dashed ellipses are the projected uncertainties at the HL-LHC [103] (*magenta*) and the ILC [102] (*green* and *orange*) of the measurements of the coupling modifiers at the 68% confidence level, assuming that no deviation from the SM prediction will be found (more details in the text). We also show with the dottet black lines the 1σ ellipses of the current measurements from CMS [91] and ATLAS [90].

be significantly reduced by the expected constraints from the HL-LHC and the ILC. For instance, the uncertainty of the coupling to b-quarks will shrink below 4% at the HL-LHC[3] and below 1% at the ILC. For the coupling to τ-leptons the uncertainty is expected to be at 2% at the HL-LHC. Again, the ILC could reduce this uncertainty further to below 1%. For the coupling to t-quarks, on the other hand, the ILC cannot improve substantially the expected uncertainty of the HL-LHC (but permit a model-independent analysis). Still, the HL-LHC and the ILC are expected to reduce the uncertainty by roughly a factor of three. This demonstrates that our explanation of the LEP and the CMS excesses within the N2HDM is testable indirectly using future precision measurements of the SM-like Higgs-boson couplings. Independent of the type of the N2HDM, we can see comparing both plots in Fig. 11, that there is not a single benchmark point that coincides with the SM prediction regarding the three coupling coefficients shown. This implies that, once these couplings are measured precisely by the HL-LHC and the ILC, a deviation of the SM prediction has to be measured in at least one of the couplings, if our explanation of the excesses is correct. Accordingly, if no deviation from the SM prediction regarding these couplings will be measured, our explanation would be ruled out entirely. Of course, this result is not surprising, as we explicitly demanded a lower limit on the singlet component of the SM-like Higgs boson of $\Sigma_{h_2} \geq 10\%$ in our scans. Consequently, the second lightest Higgs boson naturally exhibits deviations regarding the coupling coefficients. However, we checked explicitly by dedicated scans, as discussed above that benchmark points with $\Sigma_{h_2} < 10\%$ cannot accommodate both excesses, because in that case the doublet component of h_1 is too small. Thus, the conclusions w.r.t. the coupling analysis is not affected by demanding $\Sigma_{h_2} \geq 0.1$.

Furthermore, in case a deviation from the SM prediction will be found, the predicted scaling behavior of the coupling coefficients in the type II scenario (upper plot) and the type IV scenario (lower plot), might lead to distinct possibilities for the two models to accommodate these possible deviations. In this case, precision measurements of the SM-like Higgs boson couplings could be used to exclude one of the two scenarios. This is true for all points except the ones highlighted in yellow in Fig. 11. The yellow points are a subset of points of our scans that, if such deviations of the SM-like Higgs boson couplings will be measured, could correspond to a benchmark point of both the scan in the type II and the type IV scenario. However, note that this subset of points is confined to the diagonal lines of both plots, and thus corresponds to a very specific subset of the overall allowed parameter space. For the type II scenario, in the upper plot, the yellow points are determined by the additional constraint that $|c_{h_2 t\bar{t}}| \sim |c_{h_2 \tau\bar{\tau}}|$,

---

[3]Here one has to keep in mind the theory input required in the (HL-)LHC analysis.
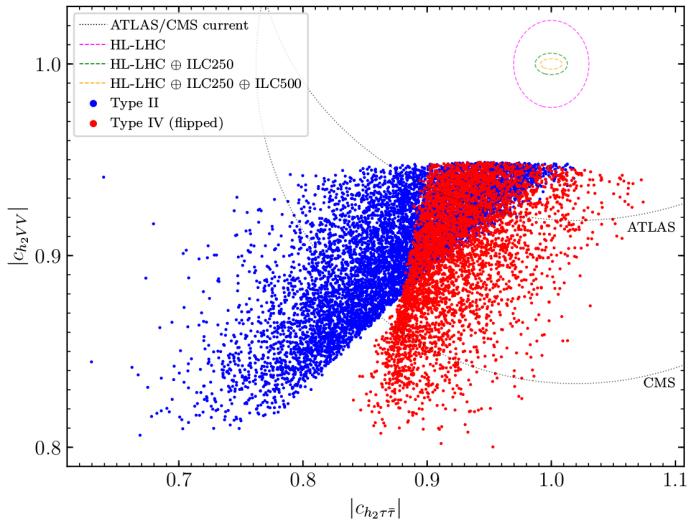
Figure 12. As in Fig. 11 but with $|c_{h_2 VV}|$ on the vertical axis.

which is exactly true in the type IV scenario. For the type IV scenario, in the lower plot, the yellow points are determined by the additional constraint that $|c_{h_2 b\bar{b}}| \sim |c_{h_2 \tau\bar{\tau}}|$, which is exactly true in the type II scenario.

For completeness we show in Fig. 12 the absolute value of the coupling modifier of the SM-like Higgs boson w.r.t. the vector boson couplings $|c_{h_2 VV}|$ on the vertical axis. Again, the parameter points of both types show deviations larger than the projected experimental uncertainty at HL-LHC and ILC. The deviations in $|c_{h_2 VV}|$ are even stronger than for the couplings to fermions. A $2\,\sigma$ deviation from the SM prediction is expected with HL-LHC accuracy. At the ILC a deviation fo more than $5\,\sigma$ would be visible. As mentioned already, a suppression of the coupling to vector bosons is explicitly expected by demanding $\Sigma_{h_2} \geq 10\%$. However, since points with lower singlet component cannot accommodate both excesses, this does not contradict the conclusion that the explanation of both excesses can be probed with high significance with future Higgs-boson coupling measurements.

5.3.2 Direct searches

Direct searches for the singlet-dominated scalar is particularly challenging at the LHC due to the large background, especially since the mass scale is close to the Z-boson resonance. In spite of that, the diphoton bump which has persisted through LHC Run I and II is worth exploring in additional Higgs boson searches of future runs of the LHC. In particular the search for charged Higgs bosons appears promising in the region of low $\tan\beta$. In Sect. 3.2 we have indicated that indeed already with the current data
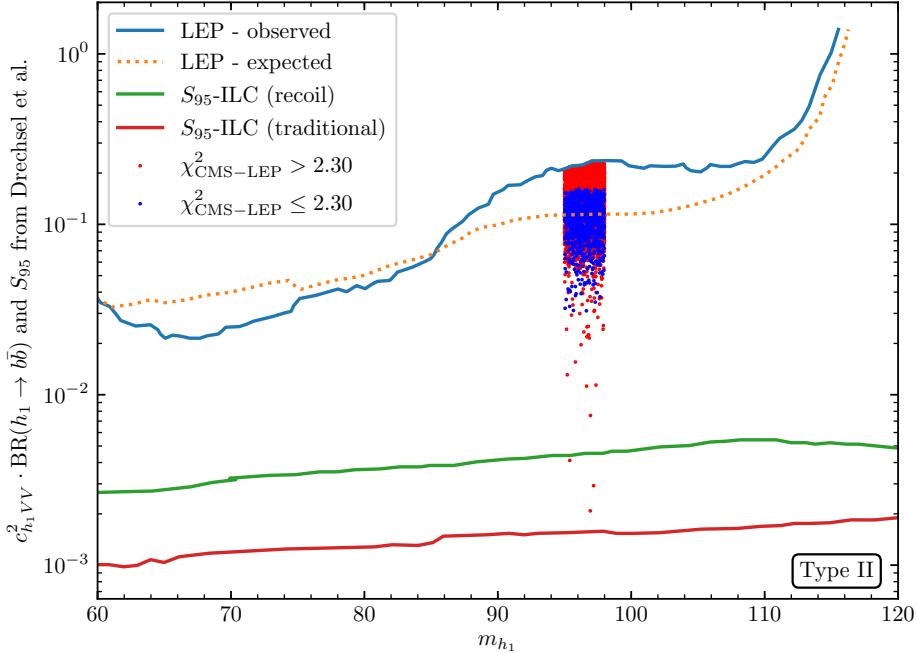
Figure 13. The 95% CL expected (*orange dashed*) and observed (*blue*) upper bounds on the Higgsstrahlung production process with associated decay of the scalar to a pair of bottom quarks at LEP [4]. Expected 95% CL upper limits on the Higgsstrahlung production process normalized to the SM prediction S_{95} at the ILC using the traditional (*red*) and the recoil technique (*green*) as described in the text [93]. We also show the points of our scan in the type II scenario which lie within (*blue*) and outside (*red*) the 1σ ellipse regarding the CMS and the LEP excesses.

the charged Higgs-boson searches with $H^{\pm} \to tb$ provide an important constraint in the favored region of parameter space. Consequently, further searches at the (HL-)LHC will yield stronger constraints or (hopefully) discover signs of a charged Higgs boson in the region between 600 GeV and 950 GeV. Prospects for a 5σ discovery in the charged Higgs-boson searches can be found in Ref. [104]. The prospects for the searches for the heavy neutral Higgs bosons, decaying dominantly to $t\bar{t}$, may also be promising. However, we are not aware of corresponding HL-LHC projections.

$e^{+}e^{-}$ colliders, on the other hand, show good prospects for the search of light scalars [93, 105]. The main production channel in the mass and energy range that we are interested in is the Higgs-strahlung process $e^{+}e^{-} \to \phi Z$, where ϕ is the scalar being searched for. The LEP collaboration has previously performed such searches [4], which resulted in the 2σ excess given by μ_{LEP}. These searches were limited by the low luminosity of LEP. However, the ILC, with its much higher luminosity and the
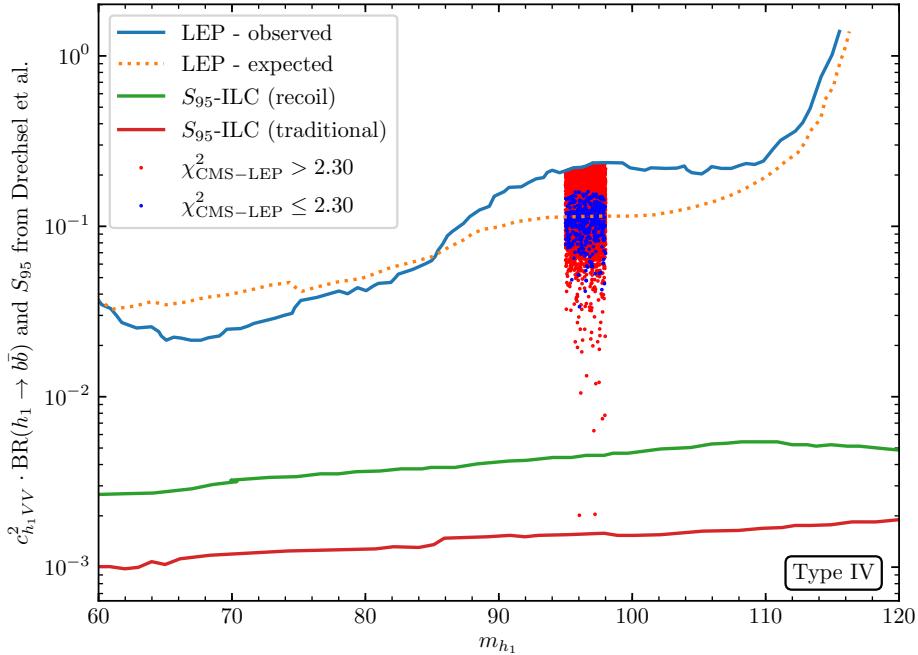
Figure 14. The same as in Fig. 13, but with the points of our scan in the type IV scenario.

possibility of using polarized beams, has a substantially higher potential to discover the light scalars. The searches performed at LEP can be divided into two categories: the 'traditional method', where studies are based on the decay mode $\phi \to b\bar{b}$ along with Z decays to $\mu^+\mu^-$ final states. This method introduces certain amount of model dependence into the analysis because of the reference to a specific decay mode of ϕ. The more model independent 'recoil technique' used by the OPAL collaboration of LEP looked for light states by analyzing the recoil mass distribution of the di-muon system produced in Z decay [106].

In Fig. 13 and Fig. 14 we show previous bounds from the LEP as well as the projected bounds from the ILC searches for light scalars in type II and type IV N2HDM scenarios respectively. The lines indicating the ILC reach for a $\sqrt{s} = 250$ GeV machine with beam polarizations (P_{e^-}, P_{e^+}) of $(-80\%, +30\%)$ and an integrated luminosity of $2000\,\text{fb}^{-1}$ are as evaluated in Ref. [93]. The quantity S_{95} used in their analysis corresponds to an upper limit at the 95% confidence level on the cross section times branching ratio generated within the 'background only' hypothesis, where the cross section has been normalized to the reference SM-Higgs cross section and the BRs have been assumed to be as in the SM (with a Higgs boson of the same mass). Consequently, we take the obtained limits to be valid for the total cross section times branching ratio. The colored points shown in Fig. 13 and Fig. 14 are the points of our scans in the

type II and type IV scenario satisfying all the theoretical and experimental constraints. The plots show that the parameter points of our scans can in both cases completely be covered by searches at the ILC for additional Higgs-like scalars.

Depending on $c_{h_1 VV}$, i.e., the light Higgs-boson production cross section, the h_1 can be produced and analyzed in detail at the ILC. A detailed analysis of the corresponding experimental precision of the light Higgs-boson couplings, however, is beyond the scope of this paper.

6 Conclusions

We analyzed a $\sim 3\,\sigma$ excess (local) in the diphoton decay mode at ~ 96 GeV as reported by CMS, together with a $\sim 2\,\sigma$ excess (local) in the $b\bar{b}$ final state at LEP in the same mass range. We interpret this possible signal as a Higgs boson in the 2 Higgs Doublet Model with an additional real Higgs singlet (N2HDM), where this Higgs sector corresponds to the Higgs sectors of the NMSSM or the (one-generation case) $\mu\nu$SSM (up to SUSY relations and an additional $\mathcal{CP}$-odd Higgs boson, which is not relevant in our analysis).

We include all relevant constraints in our analysis. These are theoretical constraints from perturbativity and the requirement that the minimum of the Higgs potential is a global minimum. We take into account the direct searches for additional Higgs bosons from LEP. the Tevatron and the LHC, as well as the measurements of the properties of the Higgs boson at ~ 125 GeV. We furthermore include bounds from flavor physics and from electroweak precision data.

We demonstrate that due to the structure of the couplings of the Higgs doublets to fermions only two types of the N2HDM, type II and type IV (flipped), can fit simultaneously the two excesses. On the other hand, the other two types, type I and type III (lepton specific), cannot be brought in agreement with the two excesses. Subsequently, we scanned the free parameters in the two favored versions of the N2HDM, where the results are similar in both scenarios. We find that the lowest possible values of $M_{H^\pm}$ above ~ 650 GeV and $\tan\beta$ just above 1 are favored. The reduced χ^2 from the Higgs-boson measurements is found roughly in the range $0.9 \lesssim \chi^2_{\mathrm{red}} \lesssim 1.3$. Due to the different coupling to leptons in type II and type IV, in general larger values of μ_{CMS} can be reached in the former, and the CMS excess can be fitted "more naturally" in the type II N2HDM. Incidentally, this is exactly the Higgs sector that is required by supersymmetric models.

Finally, we analyzed how the favored scenarios can be tested at future colliders. The (HL-)LHC will continue the searches/measurements in the diphoton final state. But apart from that we are not aware of other channels for the light Higgs boson

that could be accessible. Concerning the searches for heavy N2HDM Higgs bosons, particularly interesting are the prospects for charged Higgs bosons. For the low $\tan\beta$ values favored in our analysis, these searches have the best potential to discover a new heavy Higgs boson at the LHC Run III or the HL-LHC. Also the decay of the heavy neutral Higgs bosons to $t\bar{t}$ could be promising.

A future e^+e^- collider, such as the ILC, will be able to produce the light Higgs state at ~ 96 GeV in large numbers and consequently study its decay patterns. Similarly, we demonstrated that the high anticipated precision in the coupling measurements of the 125 GeV Higgs boson at the ILC (or CLIC, FCC-ee, CepC) will allow to find deviations in particular in the couplings to massive gauge bosons if the N2HDM with a ~ 96 GeV Higgs boson is realized in nature. Here a deviation of more than $2\,\sigma$ and $5\,\sigma$ at the HL-LHC and the ILC, respectively, can be anticipated.

We are eagerly awaiting updated analyses from ATLAS and CMS to clarify the validity of the excess in the diphoton channel.

Acknowledgements

References

[1] **ATLAS** Collaboration, G. Aad *et al.*, "Observation of a new particle in the search for the Standard Model Higgs boson with the ATLAS detector at the LHC", *Phys. Lett.* **B716** (2012) 1–29, `arXiv:1207.7214`.

[2] **CMS** Collaboration, S. Chatrchyan *et al.*, "Observation of a new boson at a mass of 125 GeV with the CMS experiment at the LHC", *Phys. Lett.* **B716** (2012) 30–61, `arXiv:1207.7235`.

[3] **ATLAS, CMS** Collaboration, G. Aad *et al.*, "Measurements of the Higgs boson production and decay rates and constraints on its couplings from a combined ATLAS and CMS analysis of the LHC pp collision data at $\sqrt{s} = 7$ and 8 TeV", *JHEP* **08** (2016) 045, `arXiv:1606.02266`.

[4] **LEP Working Group for Higgs boson searches, ALEPH, DELPHI, L3, OPAL** Collaboration, R. Barate *et al.*, "Search for the standard model Higgs boson at LEP", *Phys. Lett.* **B565** (2003) 61–75, `arXiv:hep-ex/0306033`.

[5] J. Cao, X. Guo, Y. He, P. Wu, and Y. Zhang, "Diphoton signal of the light Higgs boson in natural NMSSM", *Phys. Rev.* **D95** (2017), no. 11, 116001, `arXiv:1612.08522`.

[6] A. Azatov, R. Contino, and J. Galloway, "Model-Independent Bounds on a Light Higgs", *JHEP* **04** (2012) 127, `arXiv:1202.3415`, [Erratum: JHEP04,140(2013)].

[7] **CMS** Collaboration, A. M. Sirunyan *et al.*, "Search for a standard model-like Higgs boson in the mass range between 70 and 110 GeV in the diphoton final state in proton-proton collisions at $\sqrt{s} = 8$ and 13 TeV", *Submitted to: Phys. Lett.*, 2018 `arXiv:1811.08459`.

[8] **CMS** Collaboration, "Search for new resonances in the diphoton final state in the mass range between 80 and 115 GeV in pp collisions at $\sqrt{s} = 8$ TeV", Tech. Rep. CMS-PAS-HIG-14-037, 2015.

[9] **ATLAS** Collaboration, "Search for resonances in the 65 to 110 GeV diphoton invariant mass range using 80 fb^{-1} of *pp* collisions collected at $\sqrt{s} = 13$ TeV with the ATLAS detector", Tech. Rep. ATLAS-CONF-2018-025, 2018.

[10] S. Heinemeyer and T. Stefaniak, "A Higgs Boson at 96 GeV?!", *PoS* **CHARGED2018** (2019) 016, `arXiv:1812.05864`.

[11] S. Heinemeyer, "A Higgs boson below 125 GeV?!", *Int. J. Mod. Phys.* **A33** (2018), no. 31, 1844006.

[12] P. J. Fox and N. Weiner, "Light Signals from a Lighter Higgs", *JHEP* **08** (2018) 025, `arXiv:1710.07649`.

[13] U. Haisch and A. Malinauskas, "Let there be light from a second light Higgs doublet", *JHEP* **03** (2018) 135, `arXiv:1712.06599`.

[14] F. Richard, "Search for a light radion at HL-LHC and ILC250", `arXiv:1712.06410`.

[15] L. Liu, H. Qiao, K. Wang, and J. Zhu, "A light scalar in the Minimal Dilaton Model in light of the LHC constraints", *Chin. Phys.* **C43** (2019), no. 2, 023104.

[16] T. Biekötter, S. Heinemeyer, and C. Muñoz, "Precise prediction for the Higgs-boson masses in the $\mu\nu$SSM", *Eur. Phys. J.* **C78** (2018), no. 6, 504, `arXiv:1712.07475`.

[17] F. Domingo, S. Heinemeyer, S. Paßehr, and G. Weiglein, "Decays of the neutral Higgs bosons into SM fermions and gauge bosons in the $\mathcal{CP}$-violating NMSSM", *Eur. Phys. J.* **C78** (2018), no. 11, 942, `arXiv:1807.06322`.

[18] W. G. Hollik, S. Liebler, G. Moortgat-Pick, S. Paßehr, and G. Weiglein,

"Phenomenology of the inflation-inspired NMSSM at the electroweak scale", *Eur. Phys. J.* **C79** (2019), no. 1, 75, `arXiv:1809.07371`.

[19] H. P. Nilles, "Supersymmetry, Supergravity and Particle Physics", *Phys. Rept.* **110** (1984) 1–162.

[20] H. E. Haber and G. L. Kane, "The Search for Supersymmetry: Probing Physics Beyond the Standard Model", *Phys. Rept.* **117** (1985) 75–263.

[21] S. Heinemeyer, O. Stål, and G. Weiglein, "Interpreting the LHC Higgs Search Results in the MSSM", *Phys. Lett.* **B710** (2012) 201–206, `arXiv:1112.3026`.

[22] P. Bechtle, H. E. Haber, S. Heinemeyer, O. Stål, T. Stefaniak, G. Weiglein, and L. Zeune, "The Light and Heavy Higgs Interpretation of the MSSM", *Eur. Phys. J.* **C77** (2017), no. 2, 67, `arXiv:1608.00638`.

[23] H. Bahl, E. Fuchs, T. Hahn, S. Heinemeyer, S. Liebler, S. Patel, P. Slavich, T. Stefaniak, C. E. M. Wagner, and G. Weiglein, "MSSM Higgs Boson Searches at the LHC: Benchmark Scenarios for Run 2 and Beyond", `arXiv:1808.07542`.

[24] U. Ellwanger, C. Hugonie, and A. M. Teixeira, "The Next-to-Minimal Supersymmetric Standard Model", *Phys. Rept.* **496** (2010) 1–77, `arXiv:0910.1785`.

[25] M. Maniatis, "The Next-to-Minimal Supersymmetric extension of the Standard Model reviewed", *Int. J. Mod. Phys.* **A25** (2010) 3505–3602, `arXiv:0906.0777`.

[26] J. R. Ellis, J. F. Gunion, H. E. Haber, L. Roszkowski, and F. Zwirner, "Higgs Bosons in a Nonminimal Supersymmetric Model", *Phys. Rev.* **D39** (1989) 844.

[27] D. J. Miller, R. Nevzorov, and P. M. Zerwas, "The Higgs sector of the next-to-minimal supersymmetric standard model", *Nucl. Phys.* **B681** (2004) 3–30, `arXiv:hep-ph/0304049`.

[28] S. F. King, M. Muhlleitner, and R. Nevzorov, "NMSSM Higgs Benchmarks Near 125 GeV", *Nucl. Phys.* **B860** (2012) 207–244, `arXiv:1201.2671`.

[29] F. Domingo and G. Weiglein, "NMSSM interpretations of the observed Higgs signal", *JHEP* **04** (2016) 095, `arXiv:1509.07283`.

[30] D. E. Lopez-Fogliani and C. Munoz, "Proposal for a Supersymmetric Standard Model", *Phys. Rev. Lett.* **97** (2006) 041801, `arXiv:hep-ph/0508297`.

[31] N. Escudero, D. E. Lopez-Fogliani, C. Munoz, and R. Ruiz de Austri, "Analysis of the parameter space and spectrum of the mu nu SSM", *JHEP* **12** (2008) 099, `arXiv:0810.1507`.

[32] C. Munoz, "Phenomenology of a New Supersymmetric Standard Model: The mu nu SSM", *AIP Conf. Proc.* **1200** (2010), no. 1, 413–416, `arXiv:0909.5140`.

[33] C. Muñoz, "Searching for SUSY and decaying gravitino dark matter at the LHC and Fermi-LAT with the $\mu\nu$SSM", *PoS* **DSU2015** (2016) 034, `arXiv:1608.07912`.

[34] P. Ghosh, I. Lara, D. E. Lopez-Fogliani, C. Munoz, and R. Ruiz de Austri, "Searching for left sneutrino LSP at the LHC", *Int. J. Mod. Phys.* **A33** (2018), no. 18n19, 1850110, `arXiv:1707.02471`.

[35] T. Biekötter, S. Heinemeyer, and C. Muñoz, "Precise prediction for the Higgs-boson masses in the full $\mu\nu$SSM", Tech. Rep. IFT–UAM-CSIC–19-030.

[36] C.-Y. Chen, M. Freid, and M. Sher, "Next-to-minimal two Higgs doublet model", *Phys. Rev.* **D89** (2014), no. 7, 075009, `arXiv:1312.3949`.

[37] M. Muhlleitner, M. O. P. Sampaio, R. Santos, and J. Wittbrodt, "The N2HDM under Theoretical and Experimental Scrutiny", *JHEP* **03** (2017) 094, `arXiv:1612.01309`.

[38] R. Coimbra, M. O. P. Sampaio, and R. Santos, "ScannerS: Constraining the phase diagram of a complex scalar singlet at the LHC", *Eur. Phys. J.* **C73** (2013) 2428, `arXiv:1301.2599`.

[39] K. G. Klimenko, "On Necessary and Sufficient Conditions for Some Higgs Potentials to Be Bounded From Below", *Theor. Math. Phys.* **62** (1985) 58–65, [Teor. Mat. Fiz.62,87(1985)].

[40] A. Arbey, F. Mahmoudi, O. Stål, and T. Stefaniak, "Status of the Charged Higgs Boson in Two Higgs Doublet Models", *Eur. Phys. J.* **C78** (2018), no. 3, 182, `arXiv:1706.07414`.

[41] **ATLAS** Collaboration, M. Aaboud *et al.*, "Search for charged Higgs bosons decaying into top and bottom quarks at $\sqrt{s} = 13$ TeV with the ATLAS detector", *JHEP* **11** (2018) 085, `arXiv:1808.03599`.

[42] P. Bechtle, O. Brein, S. Heinemeyer, G. Weiglein, and K. E. Williams, "HiggsBounds: Confronting Arbitrary Higgs Sectors with Exclusion Bounds from LEP and the Tevatron", *Comput. Phys. Commun.* **181** (2010) 138–167, `arXiv:0811.4169`.

[43] P. Bechtle, O. Brein, S. Heinemeyer, G. Weiglein, and K. E. Williams, "HiggsBounds 2.0.0: Confronting Neutral and Charged Higgs Sector Predictions with Exclusion Bounds from LEP and the Tevatron", *Comput. Phys. Commun.* **182** (2011) 2605–2631, `arXiv:1102.1898`.

[44] P. Bechtle, O. Brein, S. Heinemeyer, O. Stål, T. Stefaniak, G. Weiglein, and K. Williams, "Recent Developments in HiggsBounds and a Preview of HiggsSignals", *PoS* **CHARGED2012** (2012) 024, `arXiv:1301.2345`.

[45] P. Bechtle, O. Brein, S. Heinemeyer, O. Stål, T. Stefaniak, G. Weiglein, and K. E. Williams, "HiggsBounds $-$ 4: Improved Tests of Extended Higgs Sectors against

Exclusion Bounds from LEP, the Tevatron and the LHC", *Eur. Phys. J.* **C74** (2014), no. 3, 2693, `arXiv:1311.0055`.

[46] P. Bechtle, S. Heinemeyer, O. Stål, T. Stefaniak, and G. Weiglein, "Applying Exclusion Likelihoods from LHC Searches to Extended Higgs Sectors", *Eur. Phys. J.* **C75** (2015), no. 9, 421, `arXiv:1507.06706`.

[47] E. L. Berger, T. Han, J. Jiang, and T. Plehn, "Associated production of a top quark and a charged Higgs boson", *Phys. Rev.* **D71** (2005) 115012, `arXiv:hep-ph/0312286`.

[48] M. Flechl, R. Klees, M. Kramer, M. Spira, and M. Ubiali, "Improved cross-section predictions for heavy charged Higgs boson production at the LHC", *Phys. Rev.* **D91** (2015), no. 7, 075015, `arXiv:1409.5615`.

[49] C. Degrande, M. Ubiali, M. Wiesemann, and M. Zaro, "Heavy charged Higgs boson production at the LHC", *JHEP* **10** (2015) 145, `arXiv:1507.02549`.

[50] **LHC Higgs Cross Section Working Group** Collaboration, D. de Florian *et al.*, "Handbook of LHC Higgs Cross Sections: 4. Deciphering the Nature of the Higgs Sector", `arXiv:1610.07922`.

[51] **ALEPH, DELPHI, L3, OPAL, LEP** Collaboration, G. Abbiendi *et al.*, "Search for Charged Higgs bosons: Combined Results Using LEP Data", *Eur. Phys. J.* **C73** (2013) 2463, `arXiv:1301.6065`.

[52] **DELPHI** Collaboration, J. Abdallah *et al.*, "Search for charged Higgs bosons at LEP in general two Higgs doublet models", *Eur. Phys. J.* **C34** (2004) 399–418, `arXiv:hep-ex/0404012`.

[53] **DELPHI** Collaboration, P. Abreu *et al.*, "Search for charged Higgs bosons at LEP-2", *Phys. Lett.* **B460** (1999) 484–497.

[54] **L3** Collaboration, P. Achard *et al.*, "Search for charged Higgs bosons at LEP", *Phys. Lett.* **B575** (2003) 208–220, `arXiv:hep-ex/0309056`.

[55] **OPAL** Collaboration, G. Abbiendi *et al.*, "Search for Charged Higgs Bosons in e^+e^- Collisions at $\sqrt{s} = 189 - 209$ GeV", *Eur. Phys. J.* **C72** (2012) 2076, `arXiv:0812.0267`.

[56] **OPAL** Collaboration, G. Abbiendi *et al.*, "Search for Higgs bosons in e^+e^- collisions at 183-GeV", *Eur. Phys. J.* **C7** (1999) 407–435, `arXiv:hep-ex/9811025`.

[57] **OPAL** Collaboration, G. Alexander *et al.*, "Search for charged Higgs bosons using the OPAL detector at LEP", *Phys. Lett.* **B370** (1996) 174–184.

[58] **CMS** Collaboration, "Search for a pseudoscalar boson A decaying into a Z and an h boson in the llbb final state", Tech. Rep. CMS-PAS-HIG-14-011, 2014.

[59] **CMS** Collaboration, "Search for a heavy pseudoscalar boson decaying to a Z boson and a Higgs boson at sqrt(s)=13 TeV", Tech. Rep. CMS-PAS-HIG-18-005, 2018.

[60] **ATLAS** Collaboration, G. Aad *et al.*, "Search for an additional, heavy Higgs boson in the $H \to ZZ$ decay channel at $\sqrt{s} = 8$ TeV in pp collision data with the ATLAS detector", *Eur. Phys. J.* **C76** (2016), no. 1, 45, `arXiv:1507.05930`.

[61] **ATLAS** Collaboration, M. Aaboud *et al.*, "Search for heavy ZZ resonances in the $\ell^+\ell^-\ell^+\ell^-$ and $\ell^+\ell^-\nu\bar{\nu}$ final states using proton–proton collisions at $\sqrt{s} = 13$ TeV with the ATLAS detector", *Eur. Phys. J.* **C78** (2018), no. 4, 293, `arXiv:1712.06386`.

[62] **CMS** Collaboration, "Search for a new scalar resonance decaying to a pair of Z bosons in proton-proton collisions at $\sqrt{s} = 13$ TeV", Tech. Rep. CMS-PAS-HIG-17-012, 2017.

[63] **CMS** Collaboration, "Search for H/A decaying into Z+A/H, with Z to ll and A/H to fermion pair", Tech. Rep. CMS-PAS-HIG-15-001, 2015.

[64] **ALEPH, DELPHI, L3, OPAL, LEP Working Group for Higgs Boson Searches** Collaboration, S. Schael *et al.*, "Search for neutral MSSM Higgs bosons at LEP", *Eur. Phys. J.* **C47** (2006) 547–587, `arXiv:hep-ex/0602042`.

[65] R. V. Harlander, S. Liebler, and H. Mantler, "SusHi: A program for the calculation of Higgs production in gluon fusion and bottom-quark annihilation in the Standard Model and the MSSM", *Comput. Phys. Commun.* **184** (2013) 1605–1617, `arXiv:1212.3249`.

[66] R. V. Harlander, S. Liebler, and H. Mantler, "SusHi Bento: Beyond NNLO and the heavy-top limit", *Comput. Phys. Commun.* **212** (2017) 239–257, `arXiv:1605.03190`.

[67] A. Djouadi, J. Kalinowski, and M. Spira, "HDECAY: A Program for Higgs boson decays in the standard model and its supersymmetric extension", *Comput. Phys. Commun.* **108** (1998) 56–74, `arXiv:hep-ph/9704448`.

[68] J. M. Butterworth *et al.*, "THE TOOLS AND MONTE CARLO WORKING GROUP Summary Report from the Les Houches 2009 Workshop on TeV Colliders", in "Physics at TeV colliders. Proceedings, 6th Workshop, dedicated to Thomas Binoth, Les Houches, France, June 8-26, 2009". 2010. `arXiv:1003.1643`.

[69] P. Bechtle, S. Heinemeyer, O. Stål, T. Stefaniak, and G. Weiglein, "*HiggsSignals*: Confronting arbitrary Higgs sectors with measurements at the Tevatron and the LHC", *Eur. Phys. J.* **C74** (2014), no. 2, 2711, `arXiv:1305.1933`.

[70] O. Stål and T. Stefaniak, "Constraining extended Higgs sectors with HiggsSignals", *PoS* **EPS-HEP2013** (2013) 314, `arXiv:1310.4039`.

[71] P. Bechtle, S. Heinemeyer, O. Stål, T. Stefaniak, and G. Weiglein, "Probing the

Standard Model with Higgs signal rates from the Tevatron, the LHC and a future ILC", *JHEP* **11** (2014) 039, arXiv:1403.1582.

[72] See: https://higgsbounds.hepforge.org/downloads.html.

[73] T. Enomoto and R. Watanabe, "Flavor constraints on the Two Higgs Doublet Models of Z_2 symmetric and aligned types", *JHEP* **05** (2016) 002, arXiv:1511.05066.

[74] M. Ciuchini, G. Degrassi, P. Gambino, and G. F. Giudice, "Next-to-leading QCD corrections to $B \to X_s \gamma$: Standard model and two Higgs doublet model", *Nucl. Phys.* **B527** (1998) 21–43, arXiv:hep-ph/9710335.

[75] T. Hermann, M. Misiak, and M. Steinhauser, "$\bar{B} \to X_s \gamma$ in the Two Higgs Doublet Model up to Next-to-Next-to-Leading Order in QCD", *JHEP* **11** (2012) 036, arXiv:1208.2788.

[76] M. Misiak *et al.*, "Updated NNLO QCD predictions for the weak radiative B-meson decays", *Phys. Rev. Lett.* **114** (2015), no. 22, 221801, arXiv:1503.01789.

[77] A. J. Buras, P. Krawczyk, M. E. Lautenbacher, and C. Salazar, "B0 - Anti-B0 Mixing, CP Violation, $K^+ \to \pi^+ \nu \bar{\nu}$ and $B \to K\gamma X$ in a Two Higgs Doublet Model", *Nucl. Phys.* **B337** (1990) 284–312.

[78] V. D. Barger, J. L. Hewett, and R. J. N. Phillips, "New Constraints on the Charged Higgs Sector in Two Higgs Doublet Models", *Phys. Rev.* **D41** (1990) 3421–3441.

[79] Q. Chang, P.-F. Li, and X.-Q. Li, "$B_s^0 - \bar{B}_s^0$ mixing within minimal flavor-violating two-Higgs-doublet models", *Eur. Phys. J.* **C75** (2015), no. 12, 594, arXiv:1505.03650.

[80] X.-Q. Li, J. Lu, and A. Pich, "$B_{s,d}^0 \to \ell^+\ell^-$ Decays in the Aligned Two-Higgs-Doublet Model", *JHEP* **06** (2014) 022, arXiv:1404.5865.

[81] X.-D. Cheng, Y.-D. Yang, and X.-B. Yuan, "Revisiting $B_s \to \mu^+\mu^-$ in the two-Higgs doublet models with Z_2 symmetry", *Eur. Phys. J.* **C76** (2016), no. 3, 151, arXiv:1511.01829.

[82] M. E. Peskin and T. Takeuchi, "A New constraint on a strongly interacting Higgs sector", *Phys. Rev. Lett.* **65** (1990) 964–967.

[83] M. E. Peskin and T. Takeuchi, "Estimation of oblique electroweak corrections", *Phys. Rev.* **D46** (1992) 381–409.

[84] W. Grimus, L. Lavoura, O. M. Ogreid, and P. Osland, "The Oblique parameters in multi-Higgs-doublet models", *Nucl. Phys.* **B801** (2008) 81–96, arXiv:0802.4353.

[85] S. Bertolini, "Quantum Effects in a Two Higgs Doublet Model of the Electroweak Interactions", *Nucl. Phys.* **B272** (1986) 77–98.

[86] W. Hollik, "Nonstandard Higgs Bosons in SU(2) X U(1) Radiative Corrections", *Z. Phys.* **C32** (1986) 291.

[87] G. Funk, D. O'Neil, and R. M. Winters, "What the Oblique Parameters S, T, and U and Their Extensions Reveal About the 2HDM: A Numerical Analysis", *Int. J. Mod. Phys.* **A27** (2012) 1250021, `arXiv:1110.3812`.

[88] S. Gascon-Shotkin, "Update on Higgs searches below 125 GeV". *Higgs Days at Sandander 2017,* `https://indico.cern.ch/event/666384/contributions/2723427/`.

[89] **LHC Higgs Cross Section Working Group** Collaboration, S. Heinemeyer *et al.*, "Handbook of LHC Higgs Cross Sections: 3. Higgs Properties", `arXiv:1307.1347`.

[90] **ATLAS** Collaboration, "Combined measurements of Higgs boson production and decay using up to 80 fb^{-1} of proton–proton collision data at $\sqrt{s} = 13$ TeV collected with the ATLAS experiment", Tech. Rep. ATLAS-CONF-2018-031, Jul 2018.

[91] **CMS** Collaboration, A. M. Sirunyan *et al.*, "Combined measurements of Higgs boson couplings in proton-proton collisions at $\sqrt{s} = 13$ TeV", *Submitted to: Eur. Phys. J.*, 2018 `arXiv:1809.10733`.

[92] S. Dawson *et al.*, "Working Group Report: Higgs Boson", in "Proceedings, 2013 Community Summer Study on the Future of U.S. Particle Physics: Snowmass on the Mississippi (CSS2013): Minneapolis, MN, USA, July 29-August 6, 2013". 2013. `arXiv:1310.8361`.

[93] P. Drechsel, G. Moortgat-Pick, and G. Weiglein, "Sensitivity of the ILC to light Higgs masses", in "International Workshop on Future Linear Collider (LCWS2017) Strasbourg, France, October 23-27, 2017". 2018. `arXiv:1801.09662`.

[94] **CMS** Collaboration, "Projected Performance of an Upgraded CMS Detector at the LHC and HL-LHC: Contribution to the Snowmass Process", in "Proceedings, 2013 Community Summer Study on the Future of U.S. Particle Physics: Snowmass on the Mississippi (CSS2013): Minneapolis, MN, USA, July 29-August 6, 2013". 2013. `arXiv:1307.7135`.

[95] **CMS, ATLAS** Collaboration, A. Tricomi, "Prospects of the high luminosity LHC from ATLAS and CMS", *PoS* **EPS-HEP2015** (2015) 121.

[96] **ATLAS** Collaboration, "Projections for measurements of Higgs boson signal strengths and coupling parameters with the ATLAS detector at a HL-LHC", Tech. Rep. ATL-PHYS-PUB-2014-016, Oct 2014.

[97] M. Slawinska, "High-luminosity LHC prospects with the upgraded ATLAS detector", *PoS* **DIS2016** (2016) 266, `arXiv:1609.08434`.

[98] D. M. Asner *et al.*, "ILC Higgs White Paper", in "Proceedings, 2013 Community

Summer Study on the Future of U.S. Particle Physics: Snowmass on the Mississippi (CSS2013): Minneapolis, MN, USA, July 29-August 6, 2013". 2013. `arXiv:1310.0763`.

[99] H. Ono and A. Miyamoto, "A study of measurement precision of the Higgs boson branching ratios at the International Linear Collider", *Eur. Phys. J.* **C73** (2013), no. 3, 2343, `arXiv:1207.0300`.

[100] C. Dürig, K. Fujii, J. List, and J. Tian, "Model Independent Determination of HWW coupling and Higgs total width at ILC", in "International Workshop on Future Linear Colliders (LCWS13) Tokyo, Japan, November 11-15, 2013". 2014. `arXiv:1403.7734`.

[101] K. Fujii *et al.*, "Physics Case for the 250 GeV Stage of the International Linear Collider", `arXiv:1710.07621`.

[102] P. Bambade *et al.*, "The International Linear Collider: A Global Project", `arXiv:1903.01629`.

[103] **Physics of the HL-LHC Working Group** Collaboration, M. Cepeda *et al.*, "Higgs Physics at the HL-LHC and HE-LHC", `arXiv:1902.00134`.

[104] M. Guchait and A. H. Vijay, "Probing Heavy Charged Higgs Boson at the LHC", *Phys. Rev.* **D98** (2018), no. 11, 115028, `arXiv:1806.01317`.

[105] Y. Wang, J. List, and M. Berggren, "Search for Light Scalars Produced in Association with Muon Pairs for $\sqrt{s} = 250$ GeV at the ILC", in "International Workshop on Future Linear Collider (LCWS2017) Strasbourg, France, October 23-27, 2017". 2018. `arXiv:1801.08164`.

[106] **OPAL** Collaboration, G. Abbiendi *et al.*, "Decay mode independent searches for new scalar bosons with the OPAL detector at LEP", *Eur. Phys. J.* **C27** (2003) 311–329, `arXiv:hep-ex/0206022`.